NTNU

Norwegian University of
Science and Technology

# The effect of carbon and boron carbide additions in pressure assisted sintered silicon carbide

Henriette Skarpeid

Materials Technology
Submission date: June 2017
Supervisor: Kjell Wiik, IMA
Co-supervisor: Pål Runde, Saint-Gobain Ceramic Materials
Mari-Ann Einarsrud, IMA

Norwegian University of Science and Technology
Department of Materials Science and Engineering

# Preface

The work described in this master thesis has been performed at the Department of Materials Science and Engineering at the Norwegian University of Science and Technology (NTNU) during the spring of 2017. The work presented in this Master thesis is partly built on the project report "Densification of silicon carbide by hot-pressing and the effect of carbon" from the fall 2016, by the same author.

This work has been a collaboration between the Norwegian University of Science and Technology and Saint-Gobain Ceramic Materials AS, and both parties have contributed to the project. Most of the work and experiments have been executed at the Department of Materials Science at NTNU, except powder production and etching of samples, which took place at Saint-Gobain Ceramic Materials AS, Lillesand.

During that period numerous people have been involved in this project and provided me with their assistance. First of all, I would like to thank my supervisor, Professor Kjell Wiik for his time, guidance, and support and my co-supervisor Mari-Ann Einarsrud. I would also like to thank Pål Runde, R&D director at Saint-Gobain Ceramic Materials AS, Lillesand for the opportunity to work with silicon carbide in cooperation with the industry.

Further, I would like to thank Development Engineer Benoit Watremetz and R&D Engineer Kent Mogstad at Saint-Gobain for much-appreciated knowledge, advice and discussions, which has helped me gain insight into the world of silicon carbide. I would also like to thank all the technical staff at the Department of Materials Science and Engineering at NTNU for all the support with the experimental part. Lastly, I would like to thank all the members of Inorganic Materials and Ceramics Research Group for all the helpful advice I received during the semester.

# Abstract

Silicon carbide is a highly covalent ceramic, so additives like carbon and boron must be present in order to obtain a dense material during sintering.[1] The focus of this project is to investigate how the amount of carbon and boron carbide added effects the density, phase composition and mechanical properties of pressure-sintered silicon carbide. Three different commercial SiC-powders, Densitec 13H (13 $m^2g^{-1}$), Densitec 15H (15 $m^2g^{-1}$) and Densitec 13HR (13 $m^2g^{-1}$) were tested with different amounts of carbon, ranging from 0-2.5 wt%. The powders were hot-pressed at 2050°C with 20 MPa pressure for one hour. Densitec 13HR was also tested with boron carbide content from 0.2-1.7 wt%. These powders were spark plasma sintered at 2050 °C with 20 MPa pressure for 10 minutes. All samples were then polished and characterised.

Densitec 13H obtained higher density for lower carbon concentration than Densitec 15H, while Densitec 15H had the higher density when the amount of carbon exceed 1.0 wt%. The hardness measured with Vickers micro-indentation showed a similar trend. Both samples achieved densities above 98.5 % with no carbon addition, and a hardness of approximately 2750 HV. In Densitec 13H, the specific surface area is smaller than in Densitec 15H. Therefore, less carbon is consumed during sintering, and will have more carbon present on the grain boundaries, which will decrease the density and hardness.

Densitec 13H, which contains carbon black, was further compared to Densitec 13HR, with resin as carbon source. Both density and hardness measurements showed very similar values regardless of the amount of carbon. Densitec 13H had more large anisotropic grains, which increased the fracture toughness. The optimised boron carbide content based on density and mechanical properties are 0.7 wt%, which is lower than the concentration used today (1.2 wt%). The SPS-samples had considerable grain growth during sintering. The large grains affected the mechanical properties and resulted in high hardness, but low fracture toughness.

# Sammendrag

Silisiumkarbid er et meget kovalent keramisk materiale slik at tilsetningsstoffer som bor og karbon er nødvendig for å oppnå et tett materiale under sintring. Fokuset i denne oppgaven er å undersøke hvordan ulike mengder av karbon og borkarbid påvirker tettheten, fasesammensetningen og de mekaniske egenskapene til trykksintret silisiumkarbid. Tre forskjellige kommersielle SiC-pulvere, Densitec 13H (13 $m^2g^{-1}$), Densitec 15H (15 $m^2g^{-1}$) og Densitec 13HR (13 $m^2g^{-1}$), ble testet med forskjellig mengde karbon, fra 0-2,5 vekt%. Pulveret ble varmpresset ved 2050 °C med 20 MPa trykk i en time. Densitec 13HR ble også testet med borkarbidinnhold fra 0,2-1,7 vekt%. Disse pulverene ble spark plasma sintret ved 2050 °C og 20 MPa trykk i 10 minutter. Alle prøvene ble deretter polert og karakterisert.

Densitec 13H oppnådde høyere tetthet for lavere karbonkonsentrasjon, mens Densitec 15H hadde høyere tetthet da mengden karbon oversteg 1,0 vekt%. Hardheten, som ble målt med Vickers mikrohardhetsmåler, viste en lignende trend. Begge prøvene hadde tettheter over 98,5 % uten karbontilsetning og en hardhet på ca. 2750 HV. I Densitec 13H er det spesifikke overflatearealet mindre enn i Densitec 15H. Derfor blir det forbrukt mindre karbon under sintring, slik at det er mer karbon til stede på korngrensene, noe som vil redusere tettheten og de mekaniske egenskapene.

Densitec 13H, som inneholder carbon black, ble videre sammenlignet med Densitec 13HR, med resin som karbonkilde. Både tetthet og hardhetsmålinger viste svært like verdier uavhengig av mengden karbon. Densitec 13H hadde mange flere anisotropiske korn, noe som økte bruddseigheten. Det optimaliserte borkarbidinnhold basert på tetthet og mekaniske egenskaper er 0,7 vekt%, som er lavere enn konsentrasjonen som brukes i dag (1,2 vekt%). SPS-prøvene hadde betydelig kornvekst etter sintring. De store kornene påvirket de mekaniske egenskapene og resulterte i høy hardhet, men lav bruddseighet.

# Table of Contents

# Chapter 1

# Introduction

## 1.1 Background

Silicon carbide was the first natural occurrence of carbides found. It was discovered in meteorite residues by Dr. Moisson in 1893.[2] SiC was synthetically produced for the first time in 1891, by the American scientist Edward Goodrich Acheson. He tried to use electric heat to impregnate clay with carbon, and ended up with a material similar to diamond, which he called carborundum.[3] Today, the Acheson process is still used to produce SiC industrially.

Silicon carbide behaves almost like a diamond. It is not only one of the lightest, but also one of the hardest ceramic materials and has excellent thermal conductivity and low thermal expansion.[1] The combination of light weight and outstanding hardness make silicon carbides favoured material for armours for the security and defence industries. Due to its high abrasion resistance and relatively low cost, silicon carbide is used as abrasive material in a wide variety of applications. Silicon carbide is a suitable material for electronics applications due to its chemical inertness even at elevated temperatures, resistance to thermal shock and abrasion hardness. The main applications of SiC powder in the electronic industry are in the manufacture of kiln furniture and process components for the semiconductor industry, as well as electrical field grading and surge protection.[4] Other applications include diesel particle filters, anti-slip floors and in the aerospace market.

Saint-Gobain has been a pioneer in the development of SiC powders and ready-

to-press granules for the production of technical ceramics and composite materials. They also produce special tailor-made powders and RTP granules on request from their customers. Samples have been provided for this project work, made from SiC powder mixed with boron carbide and carbon black or resin.

To get the desired properties for some of these applications, the SiC-powder has to be transformed into a dense solid. This is achieved with heat treatment and the process is called sintering. Silicon carbide is a highly covalent ceramics in which the energy of vacancy formation is very high, which results in a low self-diffusion. [5] Densification of pure SiC is not possible using conventional sintering. In order to get close to theoretical density, additives such as carbon and boron must be utilized. Often, boron carbide ($B_4C$) is used as a source for boron, while carbon can be added in the form of carbon black or phenolic resin. Resin will decompose, leaving about 50 % of the mass as amorphous carbon. [6]

It is generally thought that carbon inhibits grain growth and increases the density by removing $SiO_2$ from the surface of the SiC particles, while boron increases the rate of the densifying mechanisms. [7] The mechanisms behind, however, are more unclear. The amount of additives needed must be determined experimentally as it varies between different silicon carbide powders. Research has shown that the density increases with increased carbon and boron content until a certain level where the carbon starts to form a secondary graphite phase and the density decreases. [8;6] Secondary phases and pores may reduce the mechanical properties, which could result in severe consequences for products produced with this powder.

For sintered ceramics, the mechanical properties are crucial for the use of silicon carbide. In order to tailor the properties of silicon carbide, it is highly beneficial to understand the characteristics of the additives used and how they affect the properties of the product.

## 1.2 Aim of work

The primary goal of this study is to investigate the effect of carbon and boron carbide on sintered silicon carbide. The study will look at commercial powders from Saint-Gobain Ceramic Materials where the carbon and boron carbide content are varied to see how this effects the (i) sintering properties (ii) the phase composition and (iii) the mechanical properties. Two different sources of carbon will be tested:

carbon black and phenolic resin. Based on the measured properties, the study will provide knowledge of the effect carbon sources and particle sizes of SiC have on the amount of carbon needed and the properties of the samples. All powders will also be tested without binders to see how this will influence the sintering mechanisms. Silicon carbide powders with different additive contents will be spray-dried and sintered by hot-pressing and spark plasma sintering. Techniques to be used on sintered samples are:

- Archimedes' principle in an exicator (density and porosity)
- Helium pycnometer (density and closed porosity)
- X-Ray Diffraction (phase composition)
- Scanning Electron Microscopy (microstructure and fracture mode)
- Vickers micro-indentation (hardness and fracture toughness)

The study will find the optimised carbon and boron carbide concentration for the commercial powders, which will help Saint-Gobain to customise their powders to meet the customers requirements.

# Chapter 2

# Literature Review

This chapter will provide the basics to understand sintering and the effect of additives in silicon carbide. First, there will be a brief presentation of silicon carbide in general, with a focus on the structure and mechanical properties of SiC. Thereafter, sintering will be presented, following by the effect of carbon and boron as sintering additives in silicon carbide.

## 2.1 Silicon carbide

The excellent properties are the reason why silicon carbide is desired in so many applications. These properties are discussed more in Section 2.1.2. The process used to synthesised SiC today, is the same process as Acheson invented in 1891, and is named after him. The main concept is to mix silica sand with coke in a large elongated mound and place large carbon electrodes at opposite ends. Since the discovery of silicon carbide, there have been many attempts to change the production method. The Acheson process is a highly energy-intensive process where only 10-15 % of the charge is converted into SiC. Despite the effort, 95 % of the world production is still produced by this process.[9] The Acheson process is described more detailed in Section 2.1.3.

### 2.1.1 The structure of silicon carbide

The primary SiC structure can be described as a closely packed framework of Si atoms with C atoms occupying half of the tetrahedral sites. The structure can also be explained by layers with tetrahedrons of $C_4Si$ or $Si_4C$. The possibility for polytypes arises when these layers are stacked differently. Over 200 polytypes have been found, but the most common and stable SiC polytypes are 3C, 4H, 6H and 15R.[10] The first number in the notation describes the number of layers in the repeating unit. The following letter indicates the crystal structure: C for cubic, H for hexagonal and R for rhombohedral. The cubic polytype 3C is also known as $\beta$-SiC, while the hexagonal structures are all known as $\alpha$-SiC. The different polytypes have widely ranging physical properties, which are listed in Tab. 2.1 and Tab. 2.2. The stacking sequence in 3C can be described with ABC notation. It follows that the 6H structure can be described in terms of a cubic ABC sequence where twists occur with $\pi$-rotation around [111] as twist operator. This twist is notated by a dash, and the total stacking notation will then be ABCB'A'C'. 4H and 15R are described with the stackings ABA'C' and ABCB'A'BCAC'B'CABA'C' respectively. The two most common polytypes are illustrated in VESTA and shown in Fig. 2.1.

**Table 2.1:** SiC-structures[11;12;13]

| **Property** | **3C** | **4H** | **6H** | **15R** |
|---|---|---|---|---|
| Crystal structure | Zinc blende(cubix) | Wurtzite(hexagonal) | Wurtzite(hexagonal) | Rhombohedral |
| Group of symmetry | T2d-F43m | C46v-P63mc | C46v-P63mc | C53v-R3m |
| Lattice parameter a [Å] | 4.3582 | 3.0730 | 3.0806 | 12.6910 |
| Lattice parameter c [Å] | - | 10.0530 | 15.1173 | - |

The stability of the different polytypes is still not fully understood. There is a lack of knowledge regarding the number of factors that influence the stability, but Jepps et al.[13] have discussed some of the different theories that exist. There is some inconsistency between tentative phase diagrams formed, but generally, 6H is thermodynamically stable above 2000 °C. 4H is stable between approximately 1700-2500 °C and 3C is certainly stable up to 1700 °C and maybe up to 2500 °C in non-equilibrium conditions. According to Inomata et al.[14] 2H-SiC is stable below

1400 °C, 3C between 1400 °C and 1600 °C, 4H between 1600-2100 °C, 6H above 2100 °C and 15R above 2200 °C.

It was generally thought that $\beta$-SiC is formed at lower temperatures, and transitions to $\alpha$- SiC at high temperatures. This is the case with pure silicon carbide. Some of the most recognised theories are based on the assumption that the crystals are formed by a spiral growth around a screw dislocation. The cubic polytype is the most stable at lower temperatures and other polytypes may result from the ordering of stacking faults within this structure. There is an agreement that the purity is a major factor and that impurities can cause the transformation between different polytypes.[15] Kistler-De Coppi et al.[15] has stated that the specific surface area controls the rates of transformation. This is further evidence that the transformation not only proceeds by an in situ rearrangement of the layers but also involves surface diffusion mechanisms. Jepps et al.[13] conducted experiments that showed that boron additives in hot-pressed SiC caused the transformation from $6H \rightarrow 4H$. This has also been confirmed by other experiments[15;16], but the mechanisms and kinetics involved were not determined[13]. Carbon has limited influence on phase transformations.[15] The polytypes might influence the grain morphology of sintered samples. Lee et al.[17] concluded that more elongated grains were formed by the presence of polytype 4H. Yoshimura et al.[18] saw that the abnormal grain growth happened simultaneously with the phase transformation of 6H to 4H, and that the number of 4H grains increased with temperature. The needle-like crystals of 4H is expected to exhibit considerable one-dimensional disorder, most likely caused by nucleation of stacking faults and growth of these may be governed by screw dislocations generated when boron atoms were incorporated in the crystal.[16]

### 2.1.2 Properties of the most common SiC-structures

Some of the key properties of silicon carbide are high hardness, low specific density, high thermal conductivity, chemical inertness even at elevated temperatures, low thermal expansion and excellent thermal shock resistance. Values for some of these properties are listed in Tab. 2.2. Silicon carbide is also used in semiconductor electronic devices at high temperatures. In addition, research are being conducted to use cubic SiC in solar cells by establishing a new intermediate band gap, which will increase the theoretical efficiency of solar cells.[20]

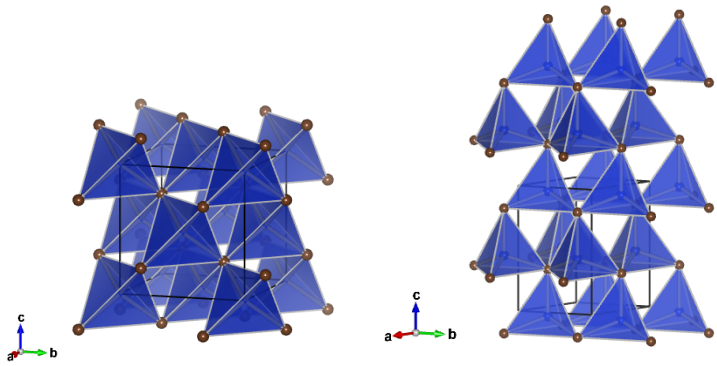


**Figure 2.1:** Illustration of the major polypes: 3C to the left and 6H to the right. The brown spheres represent carbon atoms and the blue spheres are silicon atoms.[19]

**Table 2.2:** Properties of SiC[12;11;1;4].

| **Property** | **$\alpha$-SiC (6H)** | **$\beta$-SiC (3C)** |
|---|---|---|
| Density $[gcm^{-3}]$ | 3.211 | 3.166 |
| Young's Modulus [GPa] | 448 | |
| Thermal conductivity $[WK^{-1}cm^{-1}]$ | 3.6 | 4.9 |
| Thermal expansion coefficient(300K )$[°C^{-1}]$ | $3.8{\cdot}10^{-6}$ | $4.3{\cdot}10^{-6}$ |
| Hardness [GPa] | 28.4-30.4 | |
| Fracture toughness $[MPAm^{\frac{1}{2}}]$ | 3.0-3.5 | |
| Bulk modulus [GPa] | 220 | 250 |
| Band gap [eV] | 2.390 | 3. 263 |

More of the crystal properties are listed in Tab. 2.1. As mentioned before, silicon carbide is used in abrasives because of its high hardness. On the Mohs' Hardness Scale, diamond is the hardest with a value of 10. SiC comes in as the 4th hardest material with 9-9.5, after cubic boron nitride and boron carbide. SiC is an extremely stable substance, showing no corrosion even when boiled in HCl, HF, $H_2SO_4$ or by concentrated caustic soda.[21] In air, oxidation of SiC begins at 850 °C, resulting in the formation of a $SiO_2$-film.

### 2.1.3 Production of silicon carbide

In the Acheson process, petroleum coke and silica sand, $SiO_2$, are mixed in a furnace and the overall reaction for the process is:

$$SiO_2(s) + 3C(s) \rightarrow SiC(s) + 2CO(g) \tag{2.1}$$

The furnaces used are either cylindrical or u-shaped with electrodes on both ends with current transported through the core. Quartz sand and coke are well mixed and placed around the graphite core up to the height of the electrodes. A voltage is applied and transformed into heat, which is continuously supplied from the core to the surrounding material. The temperature of the core is often in the range of 2800-3000 °C. The power is on for 45-60 hours before the furnace is cooled down for some time. The product is mostly $\alpha$-SiC, but $\beta$-SiC may be produced by the same process, but at lower temperatures.[21]

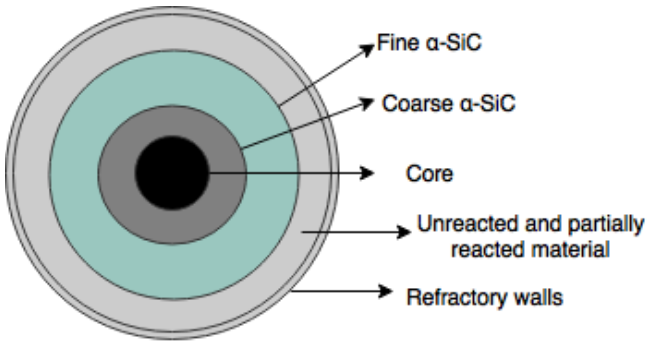


**Figure 2.2:** Illustration of the different layers of silicon carbide formed in the Acheson process.

The outer layer of material will be unreacted or partially reacted and will be reused. The next layer will be fine crystals, which is usable, but contains some impurities. The closest layer to the core will be coarse with the highest purity. These layers are illustrated in Fig. 2.2. SiC can be produced as either black or green, depending on the quality of the raw materials. The furnaces with only new material are called "green furnaces" while recycled materials are used in "black furnaces". The process is often followed by milling and chemical treatments.[1;4]

## 2.2 Mechanical properties

This subsection will provide some additional theory around the mechanical properties of silicon carbide.

### Hardness

The hardness of silicon carbide is important, since it is related to a number of other important properties or performance aspects of ceramics including compressive strength, wear, erosion and machining.[22] The reason for conducting hardness tests is further enhanced by the fact that it is obtained by a simple test that can be rapidly performed on small samples at moderate cost.

The reported hardness values of silicon carbide found varies a lot. Saint-Gobain's data-sheet in Appendix A states that the hardness is 2500 HV for sintered parts. The value has been estimated based on a 98 % dense material with some impurities. Tab. 2.2 shows the hardness of SiC was between 28.4-30.4. Other sources state that the hardness of SiC is 2800 HV[23] and 29 GPa[4].

Schaffer[23] conducted Knoop micro-hardness tests on silicon carbide crystal and found that there are significant differences between the directions in the crystal, ranging from 21 GPa in the softest, to almost 30 GPa in the hardest direction for $\alpha$-SiC. Further research by Shaffer showed that the $\beta$-phase was not significantly softer than the $\alpha$-phase, however, it did exhibit less hardness anisotropy. Sawyer et al.[24] reported that the hardness on the (0001) plane of 6H SiC varied between approximately 23.5 to 25.7 GPa as a function of orientation.

Research done by Mogstad[25] shows that hot-pressed silicon carbide will have a rather big variation in the crystallographic orientation. Analyses were done with inverse pole figure (IPF) and one image can be seen in Fig. 2.3.

It has commonly been accepted that the hardness generally increases with decreasing grain size, due to Hall-Petch type effects on the associated plastic flow, as seen in metals.[22] However, the opposite trend has been observed for ceramic materials. Hardness values obtained by Vickers micro-indentation on MgO showed that the hardness increased as the grain size increased.[26] The same trend was observed by Armstrong. et al.[27] on BeO. He concluded that the grain size can not be the primary factor determining the polycrystalline strength and that grain boundaries

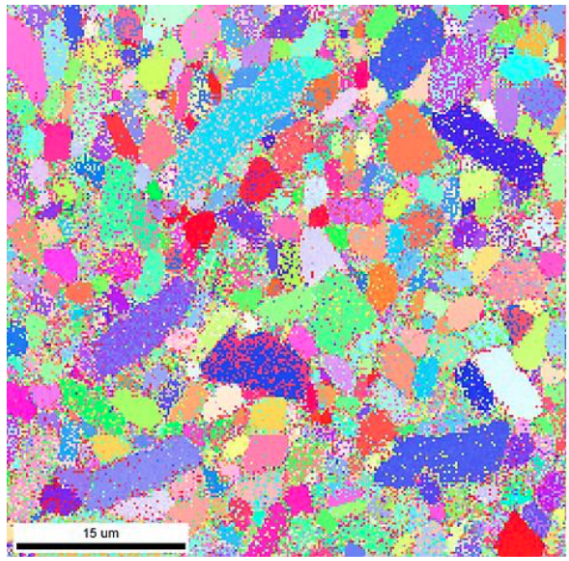


**Figure 2.3:** Inverse pole figure of SiC(2-3 wt.%C, 1.2 wt.%$B_4C$). The sample was hot-pressed for 60 minutes at 2050 °C and 20MPa. The colour changes with orientation; red is oriented with [0001] direction pointed out-of-plane, while blue and green are oriented in-plane, in the $[10\bar{1}0]$ and $[2\bar{1}\bar{1}2]$ directions, respectively.[25]

contribute to weakening of the polycrystalline material. Rice et al.[22] saw that hardness trend was to first decrease, then increase, with decreasing grain size for hard non-oxides (and oxides). It also showed a tendency to be modified by grain boundary impurities and additives, and a probable dependence on grain orientations. On the contrary, experiments conducted by Tani et al.[28] showed no grain size dependence of Vickers microhardness in $Al_2O_3$ and $Y_2O_3$, but the fracture toughness decreased with increasing grain size. Addition of sintering aids contributes to densification and hence the strength of the sintered body, but generally it also results in the formation of a second phase at the grain boundaries which frequently shows viscous fluidity at high temperatures, causing grain boundary sliding.[29]

### Fracture toughness

The fracture toughness is the resistance against crack propagation and silicon carbide has a relatively low value. The fracture toughness of SiC is approximately

3.5 MPa$\sqrt{\text{m}}$, given by Saint-Gobain Ceramic Materials. The fracture toughness obtained will also vary according to which densification additives used. Typical reported values with boron and carbon are 2.5-3.0 MPa $\sqrt{\text{m}}$, while if aluminium is used, the fracture toughness may be in the range of 3.5-4.0 MPa$\sqrt{\text{m}}$.[30]

The fracture toughness can be estimated from cracks formed during Vickers indentation. However, there are several possible methods to use and the values obtained from these can range from 2.2-5.8 MPa$\sqrt{\text{m}}$.[31] Many international studies have concluded that sharp crack techniques provide the most reliable results, where a controlled surface flaw is induced in flexure mode.[32]

The fracture toughness is influenced by the size and morphology of the grains. In non-cubic polycrystals, it has been observed that the fracture toughness increases with increasing grain size up to a critical grain size, and the toughness declines with larger grains. The general explanation is that the toughness increases as larger grains offer a stronger closure force on the crack surface and can withstand a higher displacement before fracture. However, when the grains exceed the critical value, microcracking is spontaneous, so the crack propagating connects with microcracks and the tougness decreases.[30] When it comes to morphology, several experiments[25;17;33] show that some larger, rod-shaped grains were present in hot-pressed microstructures. Elongated $\alpha$-SiC gives increased fracture toughness by crack bridging or crack deflection.[33]

The fracture can be intergranular or transgranular. Transgranular fractures ignore the grains and have smooth looking surfaces. Intergranular fractures follow the grains and take place along the grain boundaries, and leave a rougher surface with topography.

## 2.3 Sintering

Sintering is a technique where raw material, commonly a ceramic powder, is heat treated to form a compact, dense solid structure. Increased density is achieved by removing the pores between particles and form strong bonds between adjacent particles. For this to happen a source of energy must be present together with mechanisms for mass transport. Sintering is driven by a reduction in free energy for the system. The possible driving forces are a reduction in the surface free energy, applied pressure and chemical reactions.[5] When there is no chemical reactions or

externally applied pressure, the only thermodynamic driving force for sintering is a reduction of the total surface free energy of the system.

The driving force for gas phase transport is a result of differences in vapour pressure above curved surfaces. For liquid phase transport, the driving force is capillary forces due to the fact the ceramic particles are wetted by the liquid. In solid crystalline materials mass transport occurs by diffusion and the rate of diffusion depends on the temperature and the concentration of defects. The mechanism of diffusion is movement of atoms and vacancies driven by gradients in the concentration in terms of Fick's first law and occurs in the direction of decreasing chemical potential. The atoms and vacancies will have their chemical potential altered by the surface curvature. For a convex surface, the curvature is positive so the chemical potential is higher than for a flat surface. The opposite is true for a concave surface. The mass transport will happen in the direction of lowest chemical potential, the concave region. The vacancies will diffuse in opposite direction. The driving forces are illustrated in Fig. 2.4 and will with mass transport present, theoretically, result in a flat surface after some time.

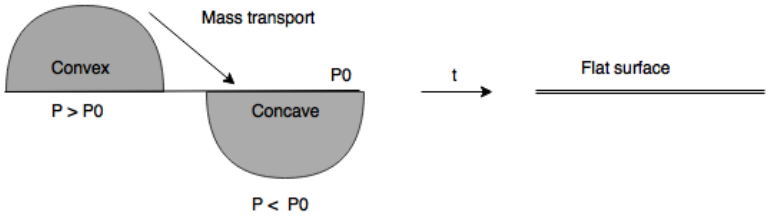


**Figure 2.4:** Illustration of how the mass transport will happen in the direction of a convex surface to a concave surface. This will theoretically result in a flat surface after some time. The driving force for gas phase transport is a difference in vapour pressure. Diffusion happens because of defect concentration differences at curved surfaces.

There is a competition between pore removal and grain growth as both lead to a reduction in the total surface surface energy of the system. The mechanisms of sintering are given in Tab. 2.3 together with information if the mechanism contributes to shrinkage or not. Densifying mechanisms result in removal of pores,

while non-densifying mechanisms result in coarsening. Non-densifying mechanisms are also important as they reduce the curvature and therefore reduces the rate of densifying mechanisms. [5]

**Table 2.3:** Mechanisms of sintering. Inspired by Rahaman. [5]

| **Mechanism** | **Source of matter** | **Densifying** | **Non-densifying** |
|---|---|---|---|
| Surface diffusion | Surface | | ✓ |
| Lattice diffusion | Surface | | ✓ |
| Vapour transport | Surface | | ✓ |
| Grain boundary diffusion | Grain boundary | ✓ | |
| Lattice diffusion | Grain boundary | ✓ | |
| Plastic flow | Dislocations | ✓ | |

The equilibrium shapes of pores in solids are determined by the balance of forces acting between the solid surface and the pore. The relationship can be described by the following equation:

$$\gamma_{GB} = 2\gamma_{SV} \cdot cos(\frac{\psi}{2}) \tag{2.2}$$

Where $\gamma_{GB}$ is the grain boundary energy, $\gamma_{sv}$ is the solid-vapor interfacial energy and $\psi$ is the dihedral angle, angle between the interfaces. This means that if a pore is surrounded by so many grains that the prescribed dihedral angle result in no curvature, i.e. flat, the driving force for pore closure is lost. If the pore surface has a concave curvature, the pore will shrink, while a convex curvature results in pore growth. The same analysis as pore shrinkage can be applied to grains in contact with each other. Flat grain boundary will give no driving force for grain growth. A small grain with a concave surface will be consumed by the surrounding grains and a large grain surrounded by many other grains will result in exaggerated grain growth and should be avoided. [34] If the grain growth rate is too fast, that is, if the grain boundary is moving faster than the vacancies, densification will not occur. The pore is trapped inside a grain and can not be removed.

There are two main types of sintering: solid-state sintering and liquid-phase sintering. Liquid-phase sintering involves the presence of a secondary phase which melts at the sintering temperature. The liquid should wet the ceramic particles

and aid rearrangement of particles and densification. In solid-state sintering, the densification is caused by solid state diffusion and makes ceramics with high purity. The different types of sintering lead to different type of properties. The sintering type chosen depends on the application.

Solid state sintering is often divided into three main stages according to the physical changes and the process is illustrated in Fig. 2.5. The initial stage involves rearrangement of particles and the formation of the first contact points, also called neck formation. The coarsening mechanisms, surface diffusion and vapor transport, will dominate this stage. There will only be up to 5% densification in this stage, so the porosity is high. Open pores will be present. In the intermediate state, most of the densification occurs. The necks between the particles grow and grain boundaries are formed. Densifying mechanisms dominate. The pores are reducing in size and at the end of the intermediate stage with around 92% of theoretical density, the pores will be closed. The pores can no longer hinder grain growth. In the final stage the grain growth occurs and the body reaches the final density. The porosity is isolated at triple points and removed by vacancy diffusion aided by movement of grain boundary and controlled grain growth. [1]

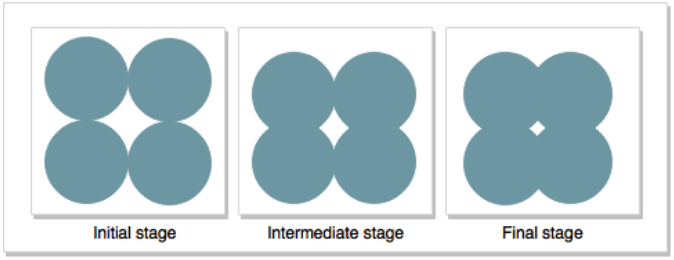


**Figure 2.5:** Illustration of the three stages of sintering; initial stage, intermediate stage and final stage.

### Hot-pressing

In conventional sintering described above, temperature is used to obtain densification. This is also referred to as pressureless sintering. Hot-pressing is analogous to pressure-less sintering except that pressure and temperature are applied simultaneously. Mechanisms for sintering also apply for hot pressing, but the densifying mechanisms are significantly enhanced. The applied pressure results in some addi-

tional driving forces such as plastic flow, rearrangement and fragmentation.[1] During the initial stage of hot-pressing, particle rearrangement is the main contributor for densification. The grains are flattened in the direction of the applied pressure. When material transport occurs by diffusion, grain boundary sliding is necessary to accommodate the change in grain shape. Other mechanisms common during hot pressing are lattice diffusion and dislocation motion.[35] The applied stress is a much greater driving force than the surface curvature, so the densification rate can be written as:

$$\frac{1}{\rho}\frac{d\rho}{dt} = \frac{HD\Phi^n}{G^m kT}P_a^n \tag{2.3}$$

where $H$ is a numerical constant, $D$ is the diffusion coefficient of the rate controlling specie, $\Phi$ is the stress intensity factor, $G$ is the grain size, $k$ is the Boltzman constant, $T$ is the temperature and the exponents depend on the mechanisms.[35] This equation can determine the densification mechanism under a set of fixed conditions.

The main advantage with hot-pressing is an increase in strength compared to pressureless sintering due to reduced porosity and less grain growth. Hot-pressing will also reduce densification time and reduce the amount of sintering additions needed, compared to pressureless sintering. However, the cost of production is high so it is only used when high density is important.[1]

### Spark Plasma Sintering

Spark plasma sintering (SPS) is a sintering technique characterized by the simultaneous application of pressure and a pulsed continuous current.[36] The current passes through the graphite die (and sample for conducting materials). The powders are heated by spark discharge between the particles and the graphite die is heated by direct current pulse voltage, so the powder is heated from both inside and outside for conduction materials, in contrast to conventional sintering and hot-pressing where the heat is provided by external elements. This makes it possible to have a very high heating rate, without damaging the equipment and sample. SPS is therefore a very fast sintering device and it is possible to have a fully sintered sample within minutes compared to hours or days with conventional sintering. In SPS, pressure and temperature are applied simultaneously. This gives high den-

sification at lower sintering temperature than pressure-less sintering, which result in less grain growth. Lower temperatures and shorter holding times have made it possible to sinter nanometric powders to near theoretical values with little grain growth.[37]

SPS is a promising sintering technique for rapid densification of advanced materials, so efforts have been made in investigating of this technique. However, limited information is available on the sintering mechanisms involved in the process. Zhaohui et al.[38] proposed the following sintering mechanisms and divided the sintering process into four stages: activation and refining of the powder, formation and growth of the sintering neck, rapid densification and plastic deformation densification. The first two stages are promoted by the spark discharge between particles, which removes the surface oxide and heats up the powder surface. Neck formations are caused by evaporation and condensation and diffusion. The third and fourth steps are promoted by the current flow through the necks which heats up the material by the Joule effect. Fast densification is promoted (third step) and enhanced by the application of the pressure (fourth step). Deformation and densification depend on the pressure and on the temperature at which it is applied.[38] In particular, the existence of spark plasma and occurrence of discharge in the sintering process is highly controversial.[39] For example, Hulbert et al.[40] gave an experimental demonstration of the absence of spark discharge and plasma during the SPS process. On the other hand, Zhang et al.[39] concluded, based on a microstructure analysis, that spark discharge does indeed occur during the SPS process.

## 2.4 Sintering of silicon carbide

Pure silicon carbide is very hard to densify as they have very strong covalent bonds.[5] These bonds inhibit vacancy diffusion which results in very slow self-diffusion. The absence of sintering in pure silicon carbide has been attributed to the high grain boundary to surface energy ratio ($\gamma_{GB}/\gamma_{SV\cdot}$). Though, $\gamma_{GB}$ is unknown, it is assumed to be high due to the strong bonds.[41] Surface diffusion and vapour transport are the dominating transport mechanisms and will therefore prevent densification.[41] Pure silicon carbide can be densified only by sintering with very high temperature and pressure. Nadeau[42] manage to get 99.5 % of theoretical

value of pure SiC by hot-pressing the samples with 2500 °C and 50 kbars. Fully dense samples(>98 %) of pure silicon carbide have also been obtained by spark plasma sintering.[43]

Sintering of silicon carbide is mainly done using additives to avoid the need for ultra-high pressure and temperature. The additives chosen depends on the sintering type. In liquid phase sintering, $Al_2O_3$, $Y_2O_3$ and MgO have been proven to be effective sintering aids.[44] The solid-state sintering additives reported for SiC include boron, carbon and aluminium.[44] Prochazka et al.[45]introduced the solid-state sintering of SiC. They added B and C as sintering additives to reduce the grain boundary-surface energy ratio, thereby inducing a driving force for the diffusional mass transport for sintering. Since then, carbon and boron as sintering aids have been a superior in solid-state sintering. When silicon carbide is sintered at 2050 °C with these additives, nearly theoretical density can be achieved.

### 2.4.1 The effect of carbon

The addition of carbon is necessary for densification of silicon carbide. Fig. 2.6 shows how density increases with increasing carbon content in an experiment conducted by Murata et al[8]. With no carbon added, the density is around 2 $gcm^{-3}$, only a small increase from the green body density. The density increases almost linearly up to approximately 2 wt% where the curve flattens out, and the maximum density is achieved around 4 wt% carbon. It was found that the grain size decreased with increasing carbon content, which implied that carbon is an effective grain growth inhibitor. Measurements done showed that that the carbon content which is effective for obtaining the maximum sintered density was independent of the type of boron compound and sintering temperature used.[8]

Another experiment conducted by Stobierski et al.[6] shows similar trends. Fig. 2.7 shows that in the case of hot pressing, the changes in density are smaller and nearly theoretical density is obtained at carbon concentration of 1.5 wt%. Even without carbon, hot-pressing gives an apparent density of almost 94 % of theoretical value. Whereas on pressureless sintering, the highest densification degree is attained at carbon concentration of 3 wt%. The fact that the density decreased above 4 wt% of carbon additive results from the appearance of secondary carbon phase in the materials, commonly located at triple junctions.[6;46] Also here the most

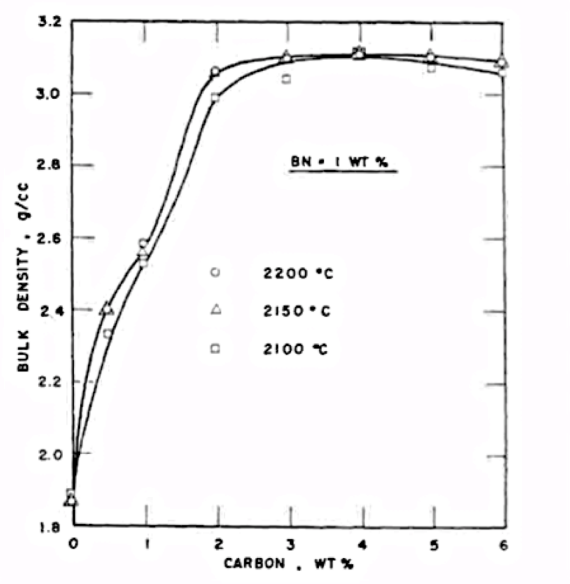


**Figure 2.6:** Measured density vs carbon content for SiC with 1 wt% of BN addition. Phenolic resin used as carbon source. Sintered for 30 minutes in an argon atmosphere. The temperature was varied from 2100-2200 °C.[8]

visible effect of increasing carbon concentration is decreased grain growth.[6] The carbon content at maximum density varies between SiC-powders and the exact relationship between density and carbon content must be determined experimentally.

Both carbon black and the phenolic resin are reported in the literature to be good sources of carbon. The phenolic resin, however, is expected to be a more effective densification agent, because it may be made more readily and uniformly available to all SiC particles.[47] Prochazka[41] investigated the effect of two different carbon sources on $\alpha$-SiC (8 $m^2g^{-1}$): carbonaceous resin and carbon black. Without any carbon, only 63 % was obtained by pressureless sintering. The addition of 0.25 wt% resin gave a final density of 96 %. However, when C was introduced as carbon black, an even higher concentration did not result in the same final density. His explanation was that it is more demanding to achieve a homogeneous distribution of carbon black and the powder demand more mixing. The reason was also related to the low carbon diffusivity in SiC, which does not allow proper carbon redistribution over the SiC surface. Hojo[48] had results supporting the conclusion

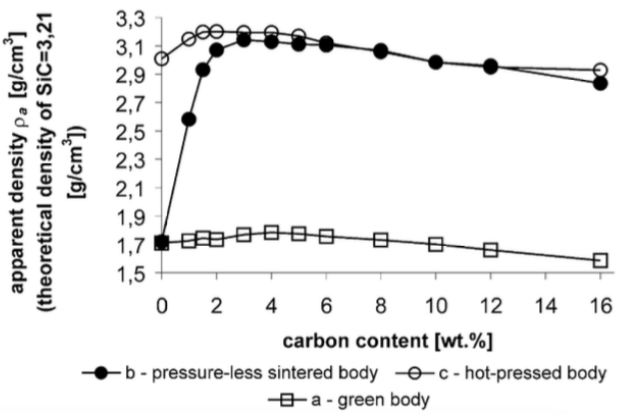


**Figure 2.7:** Apparent density for the following compounds: a)green body, b)pressure-less sintered body, c)hot-pressed body. 0.5 wt% boron is added in the samples. The pressure-less sintering was conducted at 2150 °C for 60 minutes, while the hot-pressed sample had the same temperature, but the annealing time was 30 minutes with 25 MPa pressure. Phenol-formaldehyde resin used as carbon source. [6]

that uniform addition of carbon makes a major contribution to improving the sinterability. Tanakan [49] used pitch tar, phenol resin, furan resin and carbon black as carbon sources for the samples. Carbon black resulted in the lowest densities with low carbon content, while phenol resin had a steep decline in density with content above 2 %. This was explained by that carbon black is added as a solid and is not able to diffuse into the powders as well as the other liquid materials. [49]

Prochazka [41] linked the role of carbon to the removal of silica and Si on the surface to increase the effective surface energy and promote sintering of boron doped SiC. It is assumed that carbon will remove $SiO_2$ from the surface of the SiC particles by the overall reaction

$$SiO_2\,(s) + 3\,C\,(s) \rightarrow SiC\,(s) + 2\,CO\,(g) \tag{2.4}$$

above 1520 °C . In the absent of carbon, it is possible that $SiO_2$ is reduced by itself by the following equation which is thermodynamical stable above 1870 °C.

$$2SiO_2\,(s) + SiC\,(s) \rightarrow 3SiO\,(g) + CO\,(g) \tag{2.5}$$

Another possible transport mechanism is silicon deposition through the reaction:

$$\mathrm{SiO\,(g) + SiC\,(s) \rightarrow 2Si\,(l) + CO\,(g)} \tag{2.6}$$

which has a $\Delta G = 0$ at 1950 °C, closer to the normal sintering temperature.[50] Therefore, carbon is not needed only to remove the surface silica. SiO is relatively volatile and would promote vapour transport which strongly inhibits densification and leads to coarsening. It will also form a network of pores which is hard to remove with heat treatment.[51] Gross et al.[7] concluded that without additives the presence of a wetting film of $SiO_2$ on the SiC particles reduces the thermodynamic driving force for densification allowing only microstructural coarsening to take place.

However, experiments have shown that the highest sintering density is achieved when the carbon added is just enough to remove surface $SiO_2$ and the presence of carbon promote the reaction in Eq. 2.4.[50;51] It was first thought that carbon was added to remove silica from the SiC-surface, and thereby increase the surface energy. Recently, it has been discovered that carbon also acts as a sintering aid since a certain amount of carbon is needed regardless of the oxygen concentration in the powder.[49] Datta et al.[16] had a theory that carbon was needed to reduce the oxide layer, but also to increase the diffusivity. The explanation was that carbon is needed to hinder the formation of a silicon-rich atmosphere. This would reduce the number of Si-vacancies, and thereby reduce the diffusivity of silicon. A carbon atmosphere would equalise the ratio of Si to C to unity or less than unity in silicon carbide thereby creating silicon vacancies and thus increasing bulk diffusion. For densification to occur, the mass transport of silicon and carbon should be equal. This theory is supported by Rijswijk et al.[50] and he concluded that carbon enhances the self bulk-diffusion of SiC by 2 orders of magnitude. Stobierski et al[6] did a study on the role of carbon. Fig. 2.8 shows the results of measurements of oxygen content in pure SiC and SiC with a 3 wt% addition of carbon.

As seen, carbon reduces the concentration of oxygen at temperatures lower than 1400 °C, so the initial shrinkage is most likely caused by the removal of $SiO_2$ by Eq. 2.7.[52]

$$\mathrm{SiO_2\,(s) + C\,(s) \rightarrow SiO\,(g) + CO\,(g)} \tag{2.7}$$

At higher temperatures, there is no substantial difference with the addition of carbon. This experiment proves that the role of carbon is not limited to the reaction with $SiO_2$. Thus, the reason for adding carbon may be to prevent the

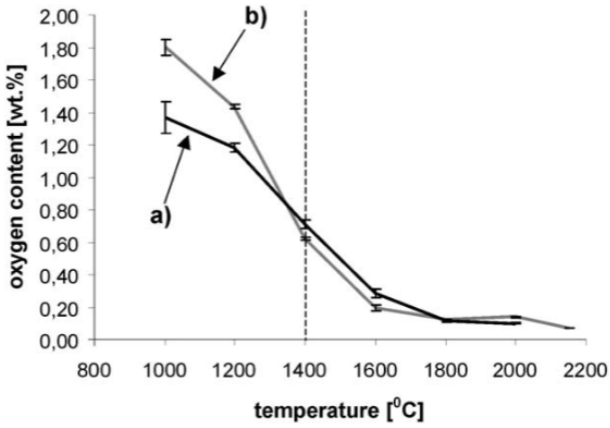


**Figure 2.8:** Changes in oxygen content for samples with a) SiC with 3 wt% carbon and b) pure SiC. [6]

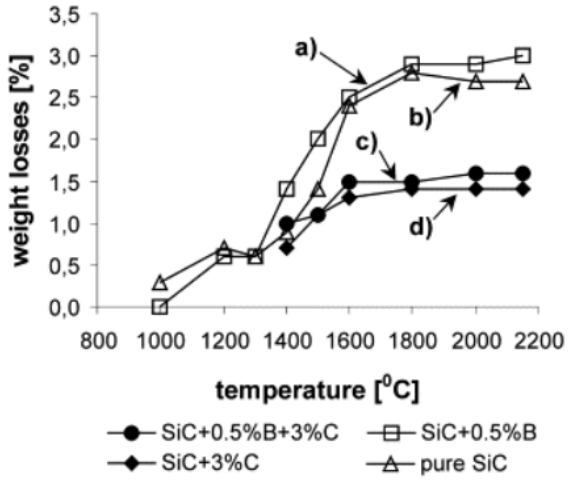


**Figure 2.9:** Weight losses for the following systems: a) pure SiC, b) SiC containing 0.5 wt% of boron, c) SiC containing 3 wt% of carbon, d) SiC containing 3 wt% of carbon and 0.5 wt% of boron. [6]

reaction between SiC and $SiO_2$, which will lead to a rapid increase in pore size. [51] Average pore radius of material containing 3 wt% of carbon is 13 times lower than in the cases with only 0.5 wt% boron addition and the one without additives, so the role of carbon is more linked to densification than boron. [6]

Carbon limits the weight loss at elevated temperatures, as seen in Fig. 2.9. The largest reduction in weight losses is found with temperatures from 1400 - 1600 °C. When C is added, the gaseous compounds, Si and $SiO_2$, can be bonded to C instead, so that CO is the only gas formed by the following equation:

$$2SiO_2(s) + nSiC(s) + 3C(s) = (n+1)SiC(s) + CO(g) \tag{2.8}$$

The densification begins at higher temperatures and Stobierski et al.[6] theory is that carbon limits those mass transport mechanisms, which are ineffective in the densification process. When these ineffective mass transport mechanisms are deactivated, already at temperatures lower than the onset of sintering, the small size of SiC grains is preserved up to the temperatures where boron activates the mass transport mechanisms leading to pore elimination.

Clegg[51], Stoberski et al.[6] and Murata[8] conducted experiments confirming that carbon significantly limits the growth of SiC grains.

### 2.4.2 The effect of boron

Boron has limited solid solubility in SiC and it is believed that the maximum concentration of boron that gives the highest density is related to the solubility limit. The solubility of boron in $\alpha$-SiC has been shown to be 0.2 wt% or less.[53] The relationship Murata et al.[8] between the density and boron carbide added is illustrated in Fig. 2.10. The figure shows that the maximum density is obtained with the use of 0.3 wt% $B_4C$ at 2100 °C and 2150 °C.

Stobierski et al.[6] found that the optimum concentration is around 0.2-0.5 wt% boron as this gives the highest density without any discontinuous growth of SiC grains or occupying surface lattice sites creating a monolayer of boron. Boron addition exceeding this point will reduce the density by segregating SiC-grains and increase the diffusion paths. The lower limit is because boron has to exceed its solubility limit in SiC to have an effect.[54] Prochazka[41] found out that boron may be introduced into SiC in the form of elemental B or $B_4C$ powder without affecting the final densities, implying that the boron diffusivity in SiC is sufficient to redistribute the element over the SiC surface during the heating up period.

The source of boron must be taken into consideration when determining the amount of additive needed. Murata et al.[8] determined the solubility limit for BN

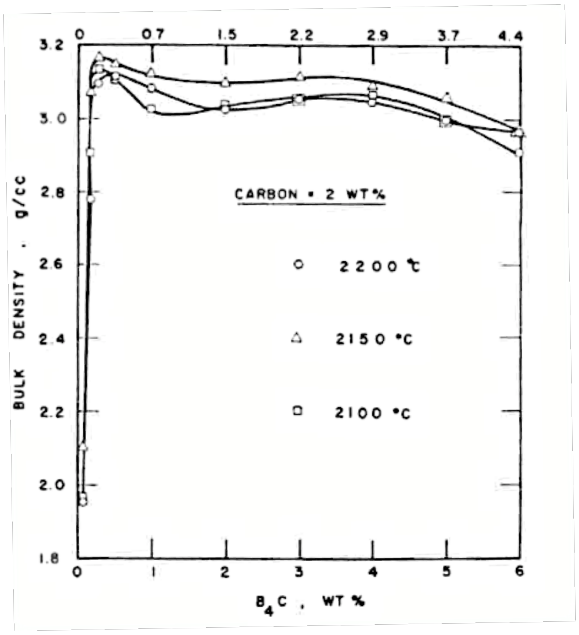


**Figure 2.10:** The relationship between density and boron carbide addition. The samples were pressure-less sintered at three different temperatures, 2100 °C, 2150 °C and 2200 °C for 30 minutes in argon atmosphere. [8]

and $B_4C$ to be 1.25 wt% and 0.5 wt%, respectively. These results were obtained at a sintering temperature of 2200 °C for 30 minutes and with a carbon concentration of 2 wt%. The maximum density of sintered SiC was achieved at the level of maximum solubility of the additive. The addition of more Boron nitride than the solubility limit gave a strong linear decline in density. The maximum density achieved with BN was lower than for $B_4C$. Boron carbide had only a small decline in density when the solubility limit was exceeded and it was constant with increasing amount of $B_4C$.

There is an agreement that adding boron will increase the density, but the mechanism behind it is more unclear. The earliest explanation was Prochazkas [41] suggestion that boron segregates to the grain boundaries and decreases the $\gamma_{GB}/\gamma_{SV}$-ratio, which increases the driving force for densification. However, later experiments showed that the dihedral angles found in both densifying and non-densifying powders were always larger than 100°, implying that densification is not limited

by energy considerations.[55] Clegg[51] conducted several experiments, clarifying that boron has no effect on the growth of pores. His suggestion is that boron increases the lattice or grain boundary diffusion coefficient. This is consistent with Gross et al.[7], who suggested that boron could either inhibit the surface diffusion and evaporation-condensation, or increase bulk or grain-boundary diffusion rates. Another hypothesis involves the formation of a liquid phase at the sintering temperature, due to observation of a second phase.[56] This theory was also proposed by Stobierski et al.[57] as a very high densification degree was attained fast, which is not possible with grain rearrangements. In contrast, Ogbuji[58] could not see any secondary or amorphous phases with high-resolution inspections of grain boundaries and concluded that liquid-phase sintering could not possible.

Boron can substitute for both silicon and carbon atoms in the lattice. It is, therefore, possible that even a small addition of boron can lower the activation energy for diffusion and increase the rate of material transport leading to densification.[54] Many researchers have looked into this theory. Datta et al.[16] concluded that B can substitute into the lattice, which would increase the diffusion. When B takes a C site, $SiB_4$ probably forms, so that Si vacancies are created. This can be described by the following Kröger-Vink notation[59], if it is assumed that SiC is an ionic compound:

$$SiB_4 \xrightarrow{SiC} 4B_C^{\cdot\cdot\cdot} + Si_{Si}^{x} + 3V_{Si}^{''''} \tag{2.9}$$

On the other hand, if B takes a Si site, C vacancies are created:

$$B_4C \xrightarrow{SiC} 4B_{Si}^{'''} + C_C^{x} + 3V_C^{\cdot\cdot\cdot\cdot} \tag{2.10}$$

$SiB_4$ is most likely to be formed, due to more similar lattice parameters, which creates Si vacancies and thus, also increase the diffusion coefficient. This is also confirmed by Tajima et al.[60] The carbon self-diffusivity is larger in pure SiC, but when boron is added, the bulk diffusion of C and B are approximately the same and equal to the grain boundary diffusion coefficient of both silicon and carbon vacancies. Boron segregation to grain boundaries has been detected by EELS analysis by Gu et al.[61]. Silicon depletion was found at the boundaries, so they concluded that boron mainly replaces silicon and bonds with carbon at the grain boundary. The role of boron was therefore said to improve the grain-boundary diffusivity while retaining covalent bonds at the grain boundaries.[61]

# Chapter 3

# Experimental

## 3.1 Powders and Apparatus

The silicon carbide powders were produced at Saint-Gobain Ceramic Materials AS Lillesand, fabricated according to the Acheson-process. The powders were spray-dried with additives, where the amount of carbon and boron carbide were varied according to Tab. 3.2 and Tab. 3.3, respectively. Densitec 13H and Densitec 13HR have a specific surface area of 13 $m^2g^{-1}$ and Densitec 15H has a specific surface area of 15 $m^2g^{-1}$. The particle size distribution of the powders are listed in Tab. 3.1. Both particle sizes, 13 $m^2g^{-1}$ and 15 $m^2g^{-1}$, were also tested without binder to exclude binder as a source of carbon, and will be refereed to with the sample names 13CB00 and 15CB00, respectively.

**Table 3.1:** Particle size distribution of the powders used.

| **Spesific surface area** [$m^2g^{-1}$] | **Particle size distribution** [$\mu$m] | | |
|---|---|---|---|
| | $D_{90}$ | $D_{50}$ | $D_{10}$ |
| 13 | 1.00-1.55 | 0.50-0.70 | 0.15-0.30 |
| 15 | 1.50 max | 0.40-0.60 | 0.15-0.28 |

Densitec 13H and 15H contain PVA as binder and other additives in addition to carbon and boron carbide. Densitec 13HR contains resin as a binder and carbon

**Table 3.2:** A list of powders tested with different carbon content and two different carbon sources. The samples 13CB0.3-13CB1.5 and 15CB0.3-15CB1.5 were tested in another project by Skarpeid[62]. All powders are sintered with hot-pressing.

| **Trade name** | **Binder** | **$B_4C$ [wt%]** | **Carbon source** | **Carbon [wt%]** | | | | | |
|---|---|---|---|---|---|---|---|---|---|
| | | | | 0.0 | 0.3 | 0.8 | 1.0 | 1.5 | 2.5 |
| Densitec 13H | PVA | 1.2 | Carbon black | 13CB0 | 13CB0.3 | 13CB0.8 | 13CB1.0 | 13CB1.5 | 13CB2.5 |
| Densitec 15H | PVA | 1.2 | Carbon black | 15CB0 | 15CB0.3 | 15CB0.8 | 15CB1.0 | 15CB1.5 | 15CB2.5 |
| Densitec 13HR | Resin | 1.2 | Resin | | 13R0.3 | 13R0.8 | 13R1.0 | 13R1.5 | |
| Densitec 13H | - | 1.2 | - | 13CB00 | | | | | |
| Densitec 15H | - | 1.2 | - | 15CB00 | | | | | |

**Table 3.3:** A list of the powders tested with different boron carbide content. The powders are sintered with spark plasma sintering.

| **Trade name** | **Binder** | **Carbon [wt%]** | **Carbon source** | **$B_4C$ [wt%]** | | | |
|---|---|---|---|---|---|---|---|
| | | | | 0.2 | 0.7 | 1.2 | 1.7 |
| Densitec 13HR | Resin | 1.0 | Resin | 13B0.2 | 13B0.7 | 13B1.2 | 13B1.7 |

source. These powders also contain other needed additives, which are confidential. The powders contain impurities such as free carbon and silicon, iron, oxygen and so on, and the total chemical analysis and the amount of impurities can be found in Appendix A. The apparatus used in this project are listed in Tab. 3.4.

## 3.2 Procedures

A brief overview of the procedures used can be found in Fig. 3.1. The silicon carbide powders were first spray-dried to form a free-flowing powder prior to sintering. The tablets were grinded to remove carbon residuals and polished to make a smooth surface. Thereafter, the densities were measured with Archimedes' and helium pycnometer. The hardness and fracture toughness were measured with Vickers indentation, the phase composition and purity were analysed with X-ray diffraction (XRD) and the microstructure was studied in Scanning Electron Microscope(SEM).

**Table 3.4:** List of apparatus used in the sintering and characterization together with their model and area of application

| Apparatus | Model | Application |
|---|---|---|
| Hot-press | Thermal Technology Inc.HP-7010G | Sintering with external pressure |
| Spark plasma sintering | SPS 825 Dr. Sinter | Sintering with external pressure |
| Helium pycnometer | Accupyc 1330 pycnometer | Measure density |
| Polishing | Struers Tegramin-20 | Surface preparation |
| Vickers indentation | Leica VMHT MOT | Measure hardness |
| XRD | D8 Advance DaVinci | Study of phase composition |
| SEM | Hitachi S-3400N | Measure crack length and fracture mode |
| SEM | Zeiss EVO MA10 | Study microstructure |

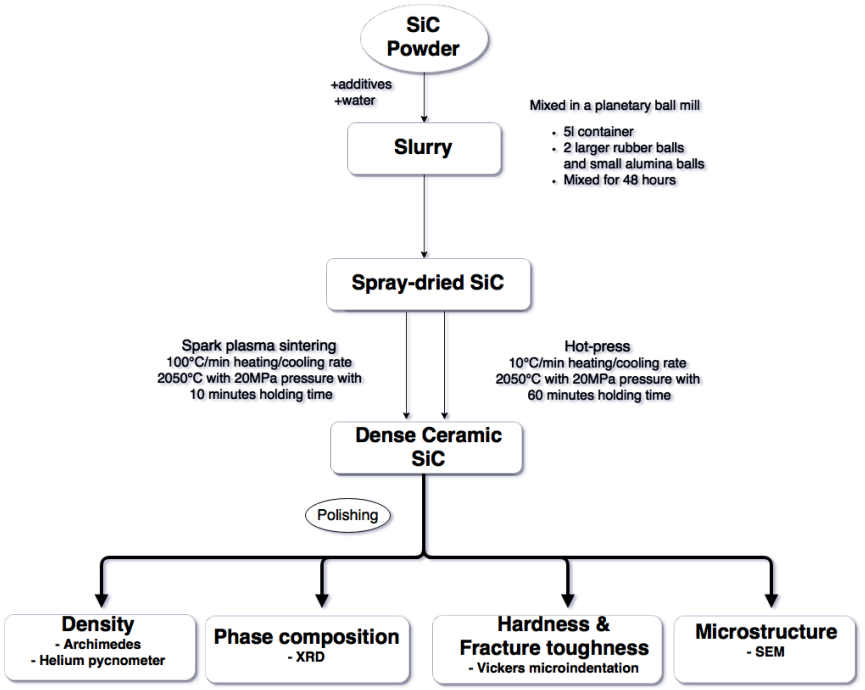


**Figure 3.1:** Flowchart of the procedures used.

### 3.2.1 Spray-drying

This process took place at Saint-Gobain Cermaic Materials and the apparatus and specific chemicals used are confidential. Prior to pressing, the silicon carbide powders were spray-dried in order to make free-flowing powders. Silicon carbide powder (2 kg) was mixed with distilled water (∼1.5 kg) and other additives given above, to form a slurry. This slurry was poured into a container made of polyethylene (5 liters). The dispersions were mixed in a planetary ball milled for minimum 48 hours with 50 rpm. Two large rubber balls and small alumina balls were used as a mixing medium. The water content and pH was checked before spray-drying. The dispersion was atomized through a nozzle to droplets of a size about 80 µm. The droplets were sprayed into a drying chamber where they were dried to form soft agglomerates and further collected in a cyclone.

### 3.2.2 Hot-press

Powder (6 g) was poured into a 2 punch graphite die (inner diameter 2.5 cm) with a graphite disk in the bottom and graphite paper at the top, to make ejection easier. See Fig. 3.2 for schematic drawing. The powder was poured into the die and the die was carefully shaken in order to have a homogeneous distribution of the powder.

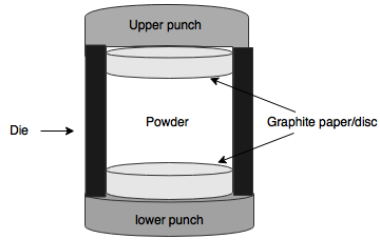


**Figure 3.2:** Schematic drawing of the sample chamber inserted into the hot-press furnace.

The die was inserted into the furnace and pressure was applied using a hydraulic pump. The chamber was evacuated three times with a rotary pump down to 3 mbar and filled with argon 5.0 (99.999 % Ar), the last time until atmospheric pressure (1 bar). A gas outlet was then opened and regulated to form a stable gas flow with a small overpressure. The furnace program was then started together with applied

pressure according to the following program. The temperature is measured with a thermocouple at low temperatures, and a pyrometer at high temperatures.

**Hot-press program**

The sintering program used in the hot-press is illustrated in Fig. 3.3. The program was started at 4.3 MPa with 10 °C/min heating rate. There was a holding time of 60 minutes at 1600 °C before 20 MPa pressure was applied and the furnace heated up to 2050 °C where there was a second holding time of 60 minutes. The system was then cooled down with a rate of 10 °C/min. The system was cooled down over night and the sintered body was removed with a uniaxial press.

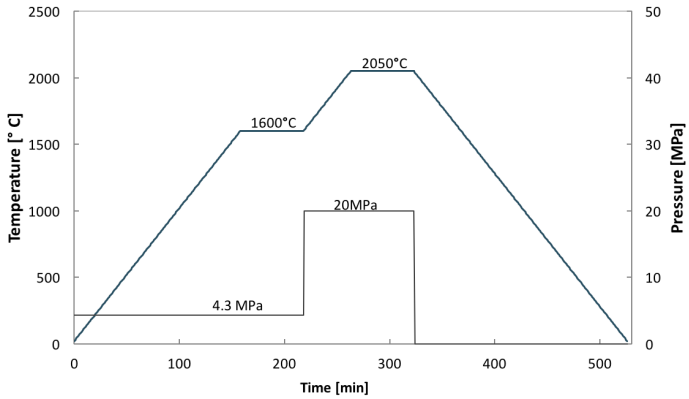


**Figure 3.3:** Illustration of the hot-press program used to sinter SiC. The cooling and heating rate is 10 °C/min and the holding times on 1600 °C and 2050 °C are 60 minutes.

### 3.2.3 Spark Plasma Sintering (SPS)

Powder (4 g) was poured into a 2 punch graphite die (inner diameter 20 mm), similar to the one used for hot-pressing. Graphite paper was shaped and placed between the graphite die and the punches/sample and two layers of graphite paper were placed at the top and bottom of the sample, making ejection easier. The powder was poured into the die before the die was carefully shaken in order to have a homogeneous distribution of the powder. The die was covered with 20 mm thick graphite wool for thermal insulation. Afterwards, the die was inserted into

the SPS with a symmetric arrangement and carefully placed in the right position with respect to the pyrometer. See Fig. 3.4 for a schematic drawing of the system. The program used for sintering is shown in Fig. 3.5.

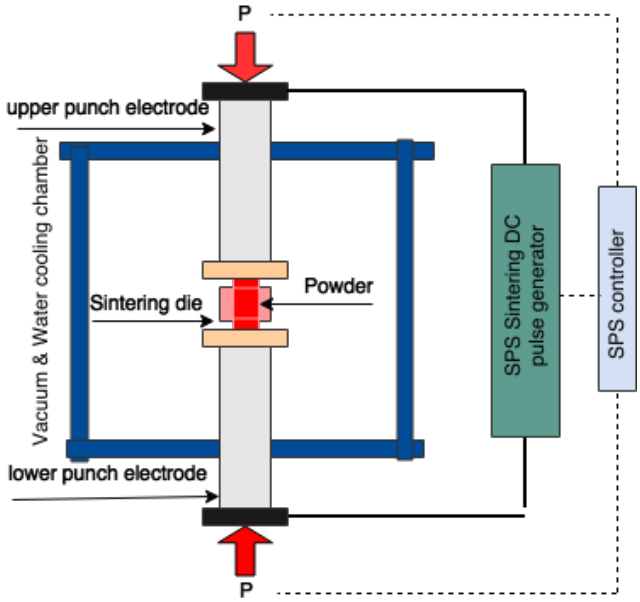


**Figure 3.4:** A schematic drawing of the Spark Plasma Sintering(SPS) method used.

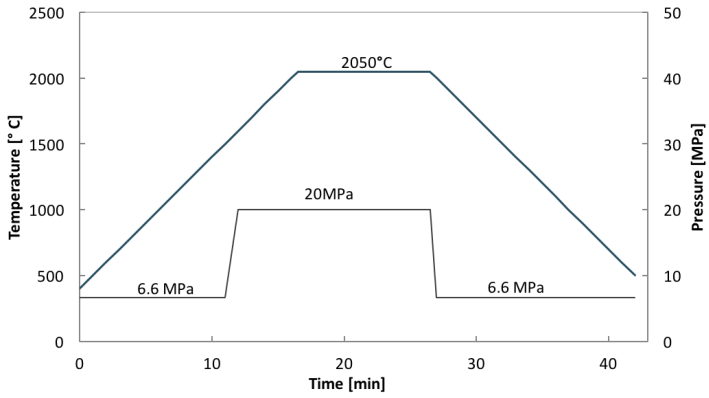


**Figure 3.5:** Illustration of the spark plasma sintering (SPS) program used to sinter SiC. The cooling and heating rate are 100 °C/min and the holding time on 2050 °C is 10 minutes.

The program was started at 6.6 MPa with 100 °C/min heating rate. At 1600 °C, a pressure of 20 MPa was applied and the furnace was further heated up to 2050 °C, where there was a holding time of 10 minutes. The system was then cooled down with a rate of 100 °C/min and the pressure were slowly reduced to 6.6 MPa. The sintered body was removed with a uniaxial press.

### 3.2.4 Surface polishing and etching

The samples were grinded to remove graphite on the surface with coarse SiC-paper (80 grit) and the first SiC-layer (0.5-1.0 mm) was removed with MD-Piano 220. The tablets were casted in epoxy and polished with the following steps:

1. MD-Piano 220, 25 N, 5 minutes, 300 rpm.
2. MD-Piano 1200, 15 N, 10-15 minutes, 150 rpm.
3. MD-Allegro, 9 µm, 15N, 10-20 minutes, 150 rpm.
4. MD-Dac, 3 µm, 10 N, 10 minutes, 150 rpm.
5. MD-Nac, 1 µm, 10 N, 5 minutes, 150 rpm.

The epoxy was removed with chloroform for further analysis of the tablets.

Kent Mogstad, at Saint-Gobain Ceramic Materials, etched the samples according to their procedure in order to look at the microstructure. KOH (50 g) and ferrocyanide (50 g) were mixed with water (100 g) in a teflon container. The mixture was heated up to the boiling point. The samples were added to the mixture for 7 minutes. If there were no structures visible in the light microscope, the sample should be in the mixture a little longer. If the samples are in the mixture for too long, the material will crack.

### 3.2.5 Phase analysis

The phase composition was analysed by X-ray diffraction. The samples were scanned in a D8 Advance Da-Vinci working in Bragg-Brentano geometry ($2\Theta - \Theta$). The diffractometer scanned from $2\Theta = 20°$-$80°$ for 60 minutes using v6. Copper $K_\alpha$ X-rays with wavelength 1.54060 nm was used. Obtained patterns were analysed in EVA software and compared against patterns found in the International

Centre for Diffraction Data (ICDD) in order to obtain phase composition. Rietveld refinement in Topas software version 5 was used for post-scanning analysis.

### 3.2.6 Density measurement

Bulk density and porosity were measured based on Archimedes' principle in an exicator.[63] The immerse liquid used was isopropanol. The weight of dry pellet ($m_1$), immersed ($m_2$) and wet ($m_3$) were measured. The equations used for calculating densities are written in Appendix B. Bulk density and closed porosity were also measured in a helium pycnometer. The sample chamber size was 10 cc and one tablet was measured at a time, so less than 10 % of the chamber volume was filled.

### 3.2.7 Mechanical properties

The hardness was measured with Vickers micro-indentation. The tests were executed on polished samples. The load used was 1 kg and 10 indents were measured per sample. The indents were taken on a straight line. The hardness can also be deduced from the contact load, $F$(kgf), and diagonal length, $d$(mm), by the following equation:

$$HV = \frac{1.854 \cdot F}{d^2} \tag{3.1}$$

An approximation of the fracture toughness, $K_{IC}$, can be derived from the crack length of the indents by the using the Anstis formula:

$$K_{IC} = 0.016 \left(\frac{E}{H}\right)^{\frac{1}{2}} \cdot \left(\frac{P}{c^{\frac{3}{2}}}\right) \tag{3.2}$$

where $E$ is the elastic modulus and $c$ is the crack length.[64] The diagonal length was based on the average value between the two directions. The crack length used for calculations was the average of four measured cracks per indent. The fracture toughness for the samples were based on 10 measurements. The lengths were measured with a Scanning Electron Microscope (SEM).

### 3.2.8 Scanning Electron Microscopy

The surfaces were examined in a Scanning Electron Microscope (SEM). The indents and cracks propagating from the indents were measured for the indents found. The fracture surfaces of the samples were also examined in SEM. The samples were fastened with a copper tape on the sample holders. The SEM parameters used are listed in Tab. 3.5.

**Table 3.5:** Scanning Electron Microscope (SEM) parameters used.

| **Parameters** | **Value** |
|---|---|
| Acc. Voltage | 10 kV |
| Working distance | 5 mm |
| Probe current | 40 nA |

# Chapter 4

# Results

In this chapter, the results from the experimental work are presented. All data of the samples 13CB0.3-13CB1.5 and 15CB0.3-15CB1.5 presented in the results is from the specialisation project by the same author [62]. It is also worth mentioning that 13R1.5 most likely has been sintered at a higher temperature than the other samples, due problems with the hot-press. First, the microstructures and density measurements are shown. Secondly, the phase composition, which is studied by X-ray diffraction. Lastly, the mechanical properties, with a focus on hardness and fracture toughness, measured with Vickers micro-indentation and Scanning Electron Microscope (SEM). The samples will be presented in the same order within each section, first the two cases with a varying carbon content with a focus on particle sizes and carbon source. Then, samples with variation boron carbide content will be presented.

## 4.1 Microstructure

The samples were etched and studied in SEM by Kent Mogstad, at Saint-Gobain Ceramic Materials. Images taken by backscatter electron detector(BSD) are shown first, followed by images taken with secondary electrons with lower magnification to detect larger grains. Photos taken of samples from the specialisation project, 13CB0.3-13CB1.5 and 15CB0.3-15CB1.5 are shown in Appendix C. From Fig. 4.1 it can be seen that the microstructures for 13CB and 15CB look similar regardless of

difference particle sizes. There is no significant difference between the samples with and without binder. It is difficult to determine exact grain size from the images, but it is very obvious that the grain size decreases with increasing carbon content. With no carbon added, most of the grains are rod-shaped. The samples with 2.5 wt% C have less elongated grains, and therefore smaller grains. There is also exaggerated grain growth present in the samples with low carbon concentration. These are anisotropic grains, and up to 400 µm long. In Fig. 4.1e, there are some black areas, which most likely are carbon rich areas.

SEM images of etched surfaces of the samples with various resin content are shown in Fig. 4.3. When the samples with resin are compared to the samples with the same amount of carbon black, Fig. C.7 in Appendix C, it looks like the average microstructures are similar. However, the samples with resin have less of the large anisotropic grains. There is one exception, 13R1.5 in 4.3d, which has very large grains as a result of a great deal of grain growth, most likely due to problems with the equipment during sintering.

The microstructures of the samples with a variation in boron carbide content are shown in Fig. 4.4. From Fig.4.4a - Fig .4.4d it is evident that all the spark plasma sintered samples have very large grains. The sample with the least boron carbide, 13B0.2 in Fig. 4.4a, has plenty of these large needle-like grains. For the rest of the samples, it looks like these needle-like grains have grown, which gives larger, more plate-shaped grains, which have grown on the behalf of the small grains in between the larger ones.

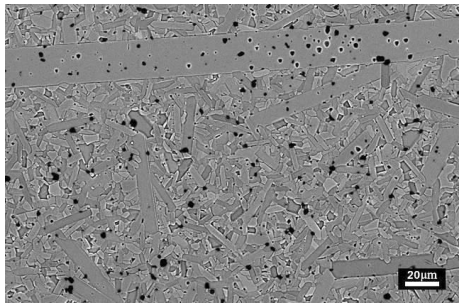


**(a)** 13CB00

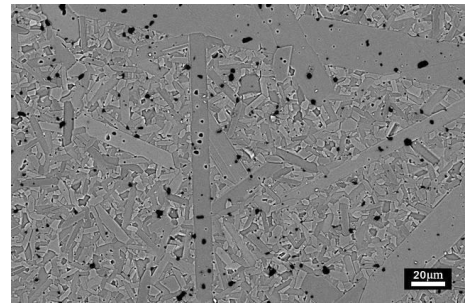


**(b)** 15CB00

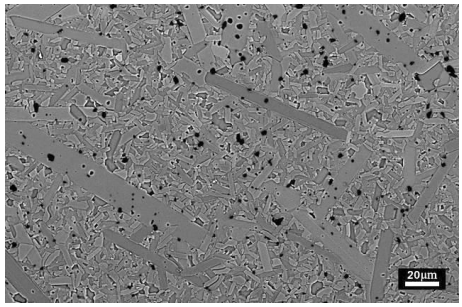


**(c)** 13CB0

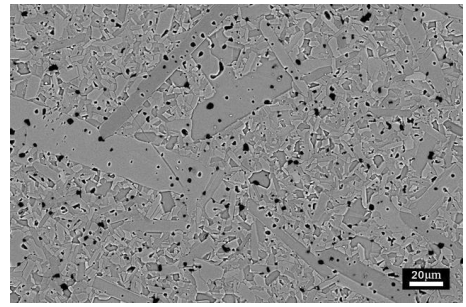


**(d)** 15CB0

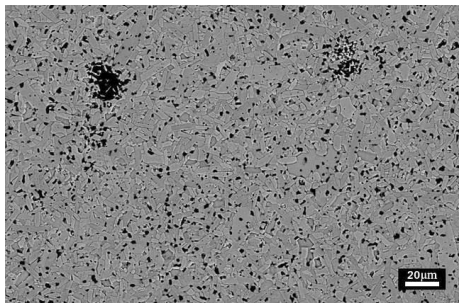


**(e)** 13CB2.5

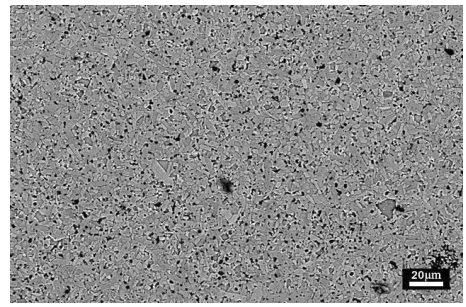


**(f)** 15CB2.5

**Figure 4.1:** BSE images of the microstructures of hot-pressed samples with different amount of carbon black and two different surface area of the SiC-powder: 13 $m^2g^{-1}$ (13CB) and 15 $m^2g^{-1}$ (15CB).

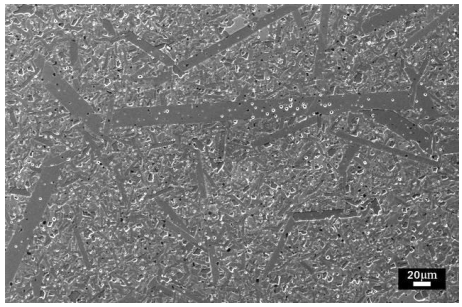


**(a)** 13CB00

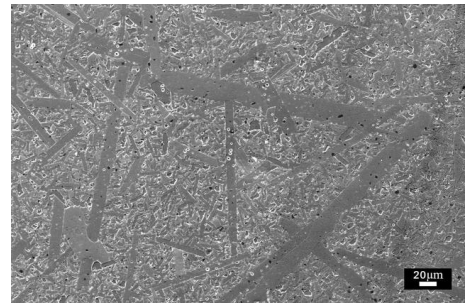


**(b)** 15CB00

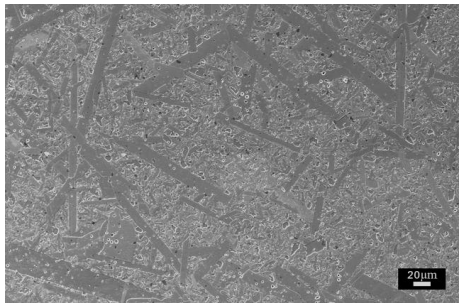


**(c)** 13CB0

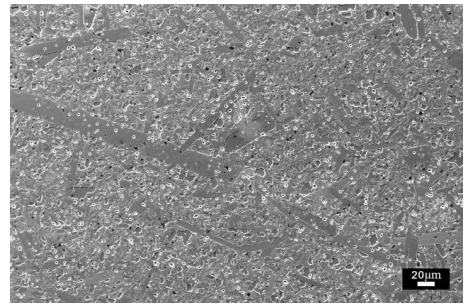


**(d)** 15CB0

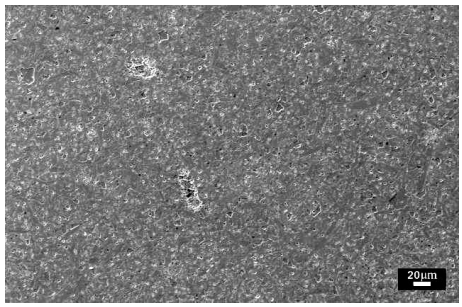


**(e)** 13CB2.5

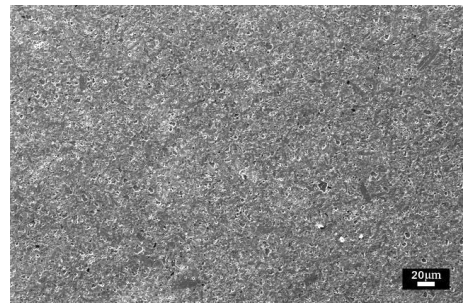


**(f)** 15CB2.5

**Figure 4.2:** SEM images of etched surfaces of the hot-pressed samples with different amount of carbon black and two different surface area of the SiC-powder: 13 $m^2g^{-1}$ (13CB) and 15 $m^2g^{-1}$ (15CB).

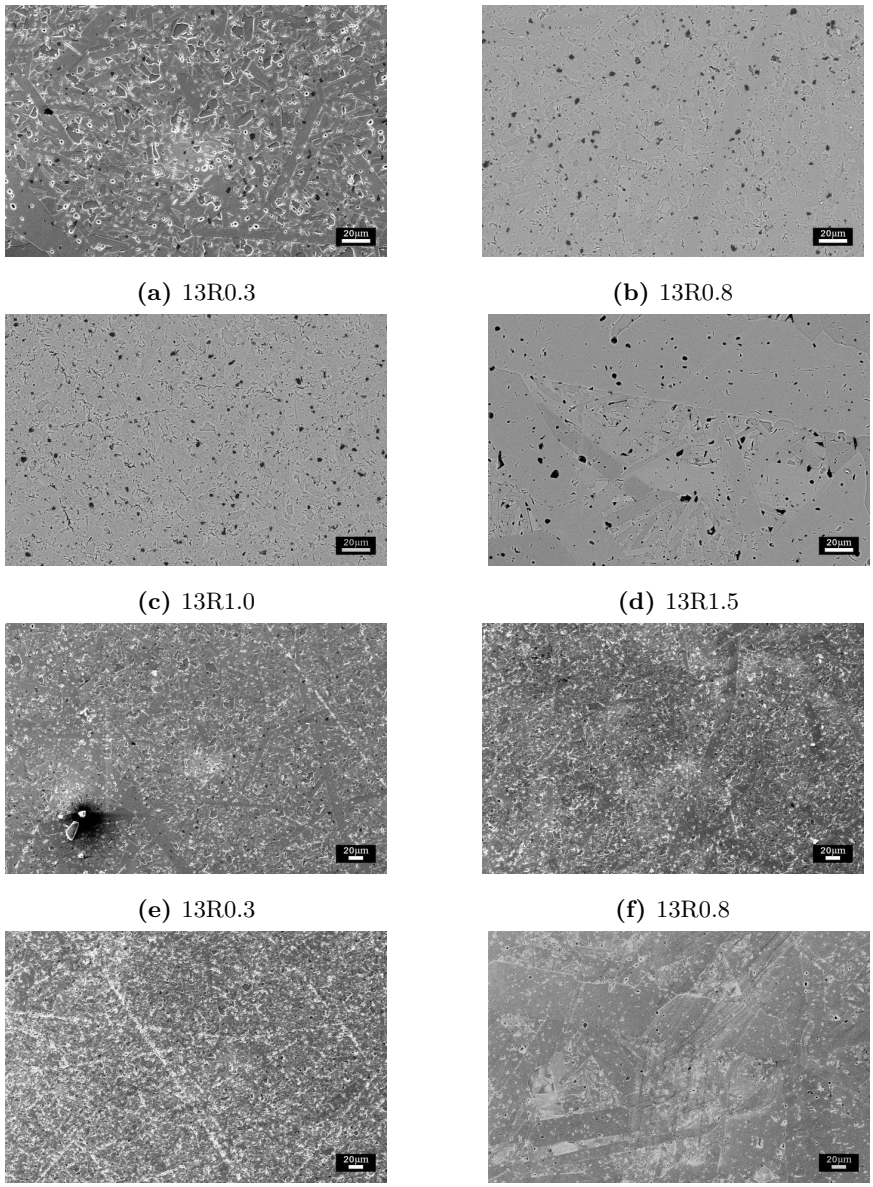


**(a)** 13R0.3 **(b)** 13R0.8

**(c)** 13R1.0 **(d)** 13R1.5

**(e)** 13R0.3 **(f)** 13R0.8

**(g)** 13R1.0 **(h)** 13R1.5

**Figure 4.3:** SEM images of etched surfaces of hot-pressed samples with variation in carbon content with resin as carbon source. The SiC-powder has a specific surface area of 13 $m^2g^{-1}$. The first four images are taken by backscatter electron detector and the bottom four are taken with secondary electrons at lower magnification.

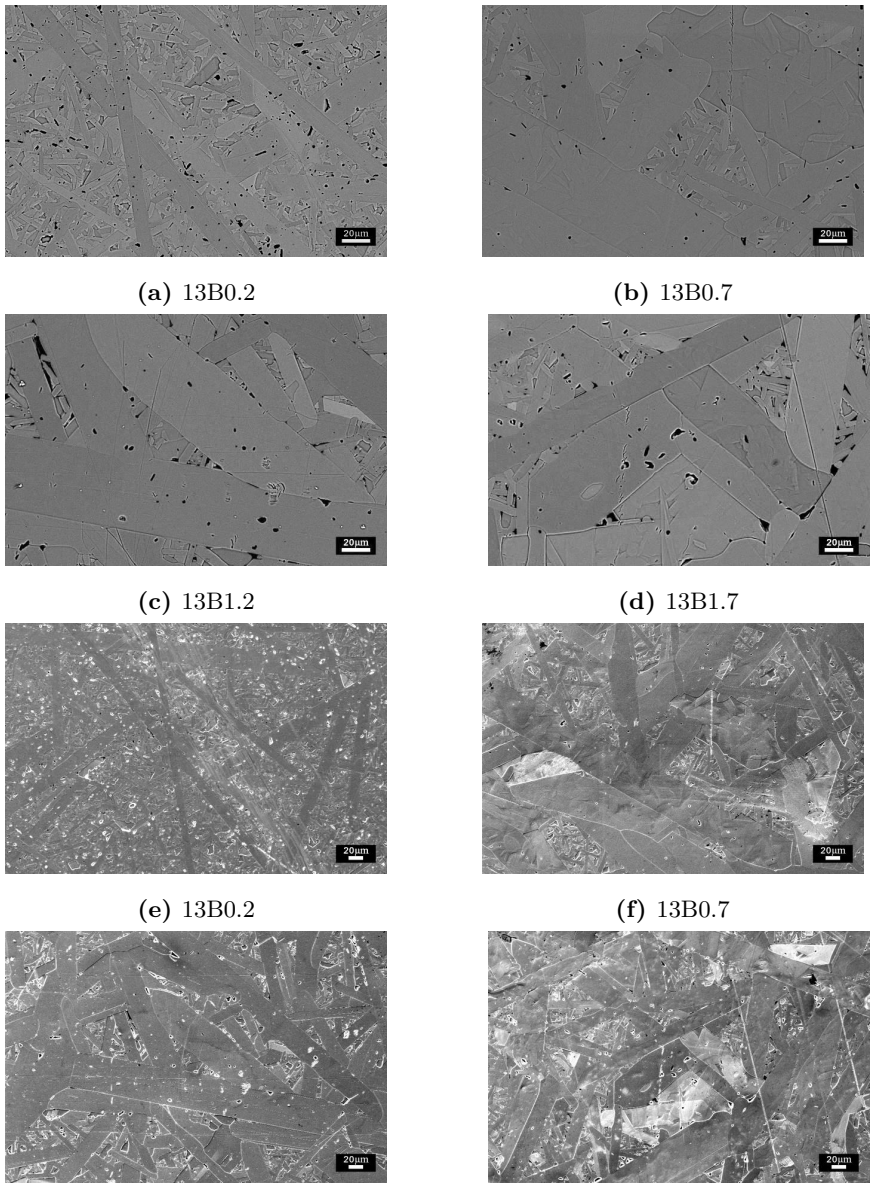


**(a)** 13B0.2 **(b)** 13B0.7

**(c)** 13B1.2 **(d)** 13B1.7

**(e)** 13B0.2 **(f)** 13B0.7

**(g)** 13B1.2 **(h)** 13B1.7

**Figure 4.4:** SEM images of the microstructure of the spark plasma sintered samples with a variation in boron carbide content and a constant amount of carbon (1.0 wt%). The SiC-powder has a specific surface area of 13 $m^2g^{-1}$. The first four images are taken by backscatter electron detector and the bottom four are taken with secondary electrons at lower magnification.

## 4.2 Density measurements

The densities measured with helium pycnometer and Archimedes' method[63] of the samples are shown in Fig. 4.5, Fig. 4.6 and Fig. 4.7. The theoretical density used, is the density of pure $\alpha$-SiC ( 3.211 $gcm^{-3}$)[12], which means that the carbon and boron carbide content have not been included in the theoretical density. The densities measured together with open and closed porosity are also listed in Tab. B.1 in Appendix B. Three density measurement were conducted on each of the 13B-samples to investigate the uncertainty in the measurements. Based on the standard deviation of the three measurements, both methods had relative equal uncertainty with a maximum value of $\pm 0.16$ % for the different samples.

Fig. 4.5 shows how the particle sizes of SiC influence the amount of carbon needed. The measurements show that all the samples have high density, even the samples without carbon and binder. The measured open porosity is less than 0.53 %, which should ideally be the difference between the two methods used. The trend is that the density increases with increasing carbon content up to a critical point, before it declines. For the 13CB-series, the critical point is between 0.8-1.0 wt% C, while it is between 1.0 wt% C and 1.5wt %C for 15CB.

Fig. 4.6 shows the density variations when two different carbon sources are used. Here, there is a difference in the trend between the two measuring methods. With helium-pycnometer, the samples with resin have lower densities than the samples with carbon black. However, based on the Archimedes' method, the densities are almost identical. The similarity between the methods is that the density clearly decreases with more than 0.5 % with 1.5 wt% C in both series. Very high densities are achieved, up to 99.4 %, taken from Fig. 4.6.

The density variations with different amount of boron carbide are shown in Fig 4.7. These samples are densified with SPS, but a sample with the same powder but densified with hot-press is included to compare the two sintering methods. The trend is that the density decreases with increasing boron carbide content. The maximum density, 98.8 % is obtained with 0.2 wt% $B_4C$. The values plotted are based on the average density of three measurements for both methods. The measurement uncertainties lie within the size of the markers. It is clear from both figures that the hot-pressed sample has higher density than the spark plasma sintered sample.

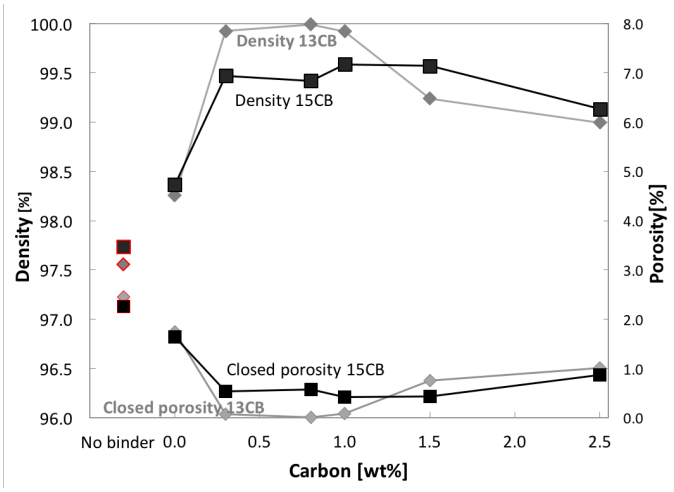


**(a)** Helium pycnometer

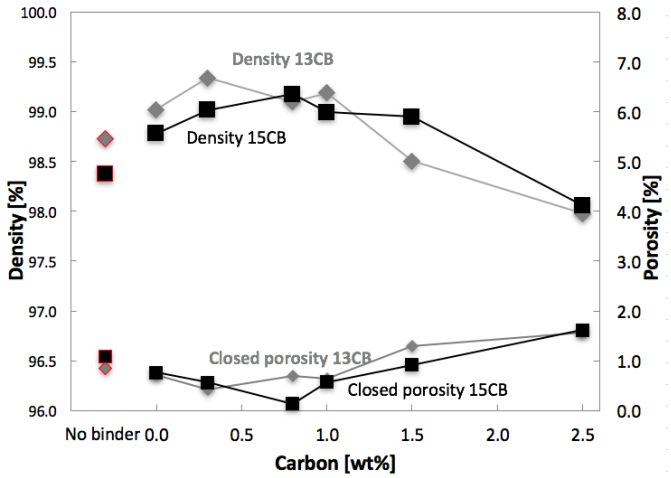


**(b)** Archimedes' method

**Figure 4.5:** Density measurements relative to the theoretical density of hot-pressed SiC with different amount of carbon. Theoretical density used is 3.211 $gcm^{-3}$.[12] Carbon black is used as carbon source in all samples, but there is a difference in the specific surface area of the powders used, 13 $m^2g^{-1}$(grey) and 15 $m^2g^{-1}$(black). The markers with red line represent the samples without binder. The two bottom lines are the measured closed porosity of the samples.

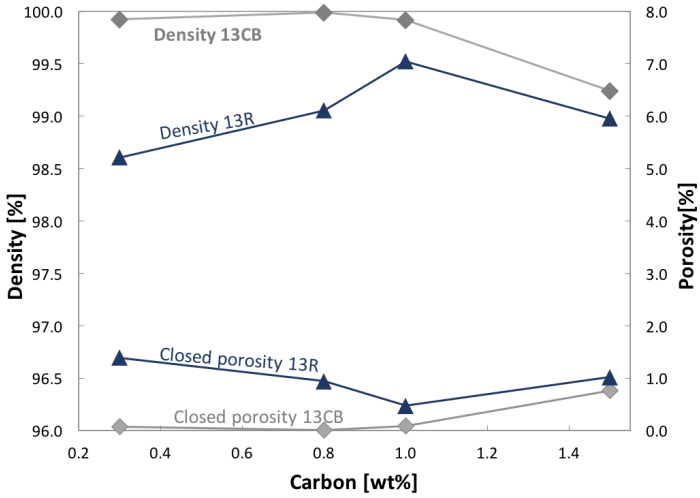


**(a)** Helium pycnometer

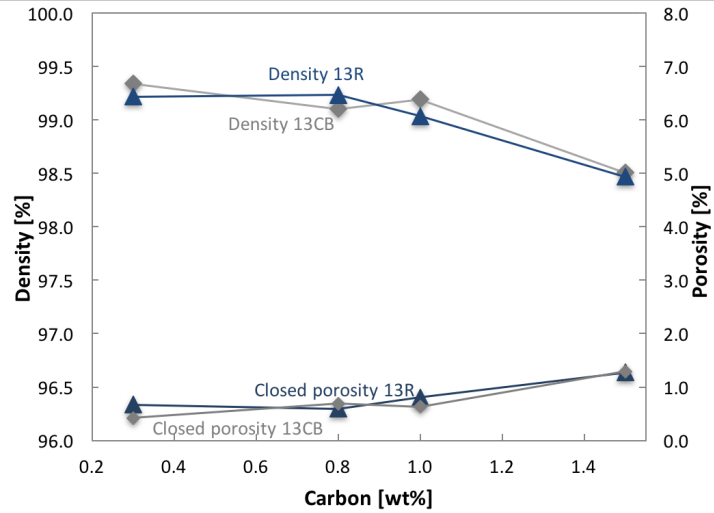


**(b)** Archimedes' method

**Figure 4.6:** Density measurements relative to the theoretical density of hot-pressed SiC with different amount of carbon. Theoretical density used is 3.211 $gcm^{-3}$.[12] The samples have the same surface area, 13 $m^2g^{-1}$, but two different sources of carbon: carbon black (grey) and resin (blue). The two bottom lines are the measured closed porosity of the samples.

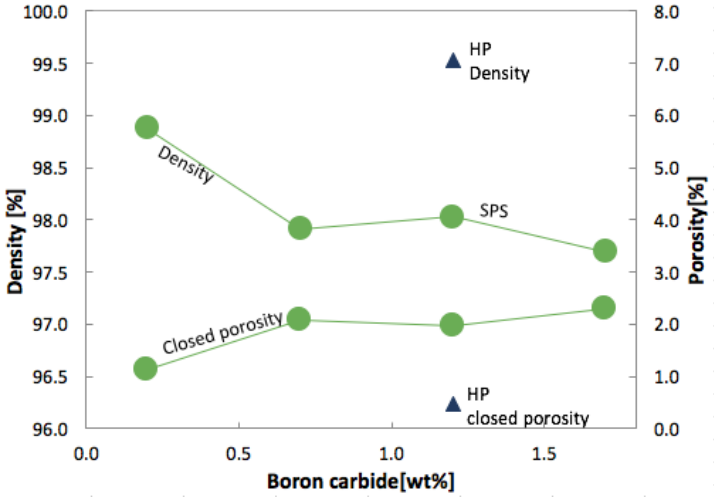


**(a)** Helium pycnometer

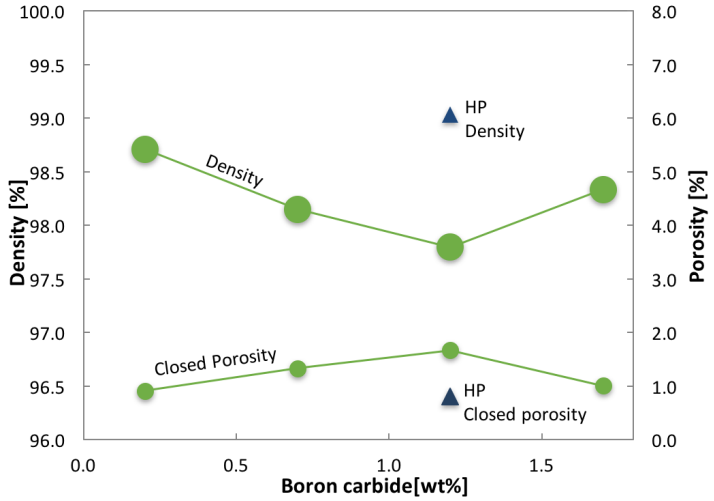


**(b)** Archimedes' method

**Figure 4.7:** Density measurements relative to the theoretical density of spark plasma sintered SiC with different amount of boron carbide added. The values are an average of three measurements and the uncertainty is the size of the marker. Theoretical density used is 3.211 $gcm^{-3}$.[12] The samples are added 1 wt% resin and 13R1.0 are plotted to compare the result from hot-pressing and spark plasma sintering (SPS).

## 4.3 Phase Compositions

The X-ray diffraction (XRD) diagram for the samples with a variation in carbon content can be found in Fig. 4.8. Fig. 4.9 shows the XRD-diagrams for the samples with variation in boron carbide content and a constant amount of carbon.

The graphite peak, marked with a triangle, increases with increasing carbon content in all samples. In 13CB-series (Fig. 4.8a), the peak is visible at 0.8 wt% C, while the phase is first clear with 1.5 wt% carbon addition in 15CB (Fig. 4.8b). In the 13R-series (Fig. 4.8c), the peak is first visible at 0.8 wt% C and when it is compared to the samples with carbon black, it is clear that it is less graphite present in the samples with resin as carbon source. The carbon peak is present in all the 13B-samples shown in Fig. 4.9, but it increases with increasing boron carbide content.

There is also some intensity variation of the different polytypes. First, if the samples with the same carbon source, but different particle sizes are compared, 15CB and 13CB, it is clear that most of the 13CB-samples have a higher intensity of the 4H diffraction lines. However, this is only the case in the samples containing carbon. The samples without carbon are very similar regardless of the difference in particle sizes. In Fig. 4.8c, the diffraction lines of the polytypes are very similar despite the use of different carbon sources with one exception. 13R1.5 has higher intensity of peaks corresponding to polytype 4H, marked with a star. There is little or no difference in the polytypes present from the XRD-diagrams in Fig. 4.9 when the boron carbide content varies.

The ratio between 4H and 6H was further examined in Topas by Rietveld structure fitting. It is assumed that 6H and 4H are the only polytypes present. The amount of 4H found in 13CB and 15CB is shown in Fig. 4.10, the amount of 4H in 13R is shown in Fig. 4.11 and the amount of 4H phase when the boron carbide content is varied is shown in Fig. 4.12. The values found are listed in Tab. B.2 in Appendix B.

The figures confirm the difference in the amount of polytypes present, as seen in the XRD-diagrams. In Fig. 4.10, there is no difference in the polytypes present when there is no carbon present. There is also a slightly decrease in the amount of 4H when the carbon content increases from 0.3 wt%. The same trend is seen in Fig. 4.11, with the exception of 13R1.5 which has a very high amount of 4H.

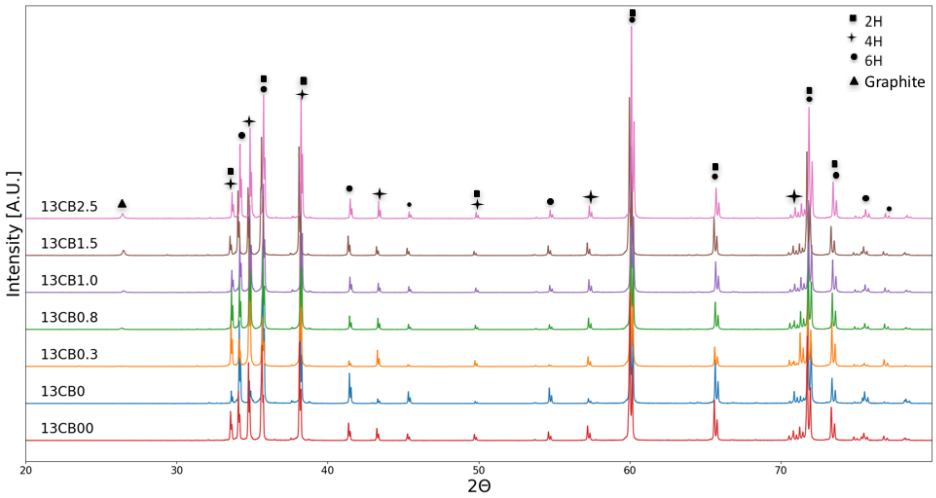


**(a)** XRD-diagrams of the samples with carbon black as carbon source and a specific surface area of 13 $m^2g^{-1}$ (13CB).

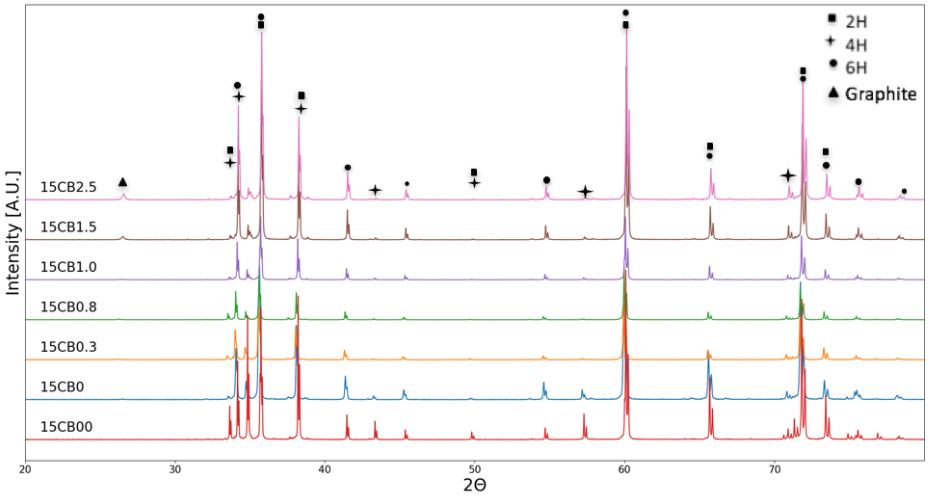


**(b)** XRD-diagrams of the samples with carbon black as carbon source and with a specific surface area of 15 $m^2g^{-1}$ (15CB).

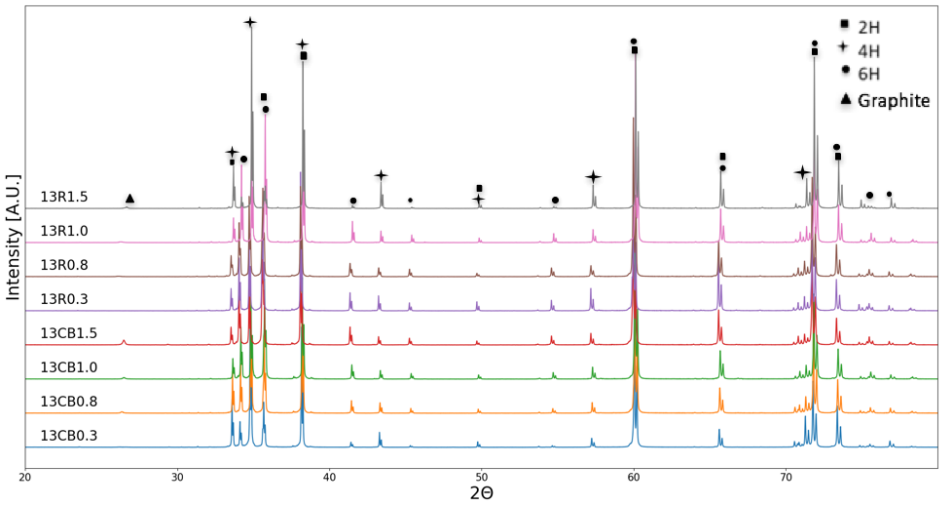


**(c)** XRD-diagrams of the samples with resin (top four) and carbon black (bottom four) as carbon source and with specific surface area of 13 $m^2g^{-1}$.

**Figure 4.8:** XRD-diagrams of the hot-pressed samples with different carbon content. The phases are found from Topas structure fitting. The star symbol represent 6H (COD 9010158), The circle is 4H (PDF 04-010-5697), the square represent 2H phase(PDF 04-010-5696), and the triangle is graphite (COD 9008569).

Fig. 4.12 confirms that the samples sintered with SPS have a high amount of 4H compared to the sample that was hot-pressed, and there are only small variations in polytype ratio as the boron carbide content changes. Two non-sintered powders were tested as well, 13CB0.3 and 15CB0.3, showing 24.07 % and 6.12 % of 4H respectively. This was carried out to give an idea of how the ration changes with different amount of carbon and the difference between the powders. The values found are not exact and may vary by up to 10 % depending on the parameters used in the structure fitting.

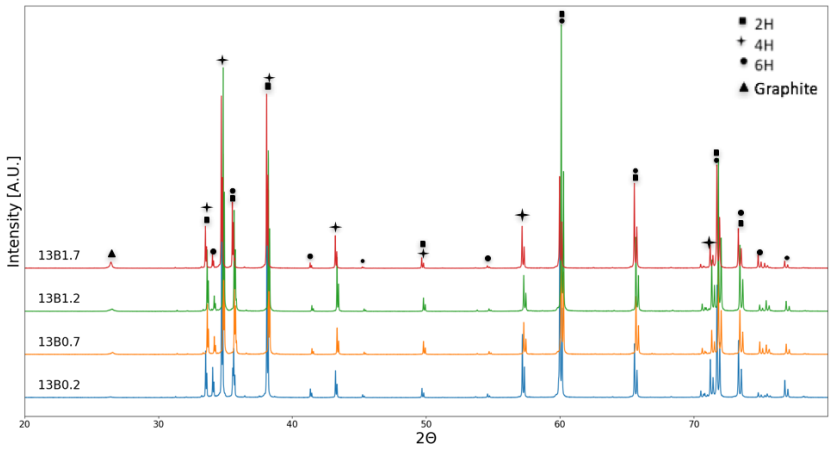


**Figure 4.9:** XRD-diagrams of the samples sintered with SPS and with variation in boron carbide content, carbon black as resin source and with specific surface area of $13 m^2 g^{-1}$ (13B). The phases are found from Topas structure fitting. The star symbol represent 6H (COD 9010158), The circle is 4H (PDF 04-010-5697), the square represent 2H phase(PDF 04-010-5696), and the triangle is graphite (COD 9008569)

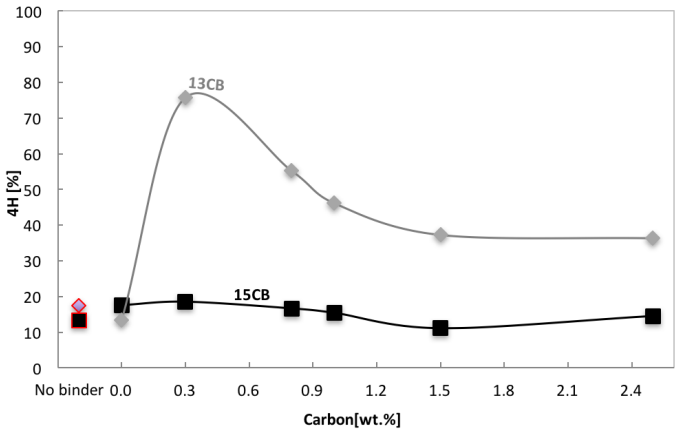


**Figure 4.10:** The amount of 4H measured by Rietveld fitting in Topas. It is assumed that 6H and 4H are the only polytypes present. The samples presented here are hot-pressed samples with carbon black, but with two different particle sizes: $13 m^2 g^{-1}$(grey) and $15 m^2 g^{-1}$(black). The red markers represent samples without binder.

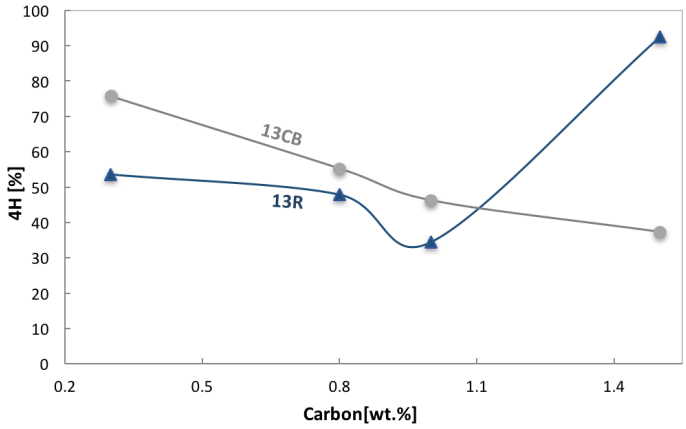


**Figure 4.11:** The amount of 4H measured by Rietveld fitting in Topas. It is assumed that 6H and 4H are the only polytypes present. The blue markers are hot-pressed samples with resin as carbon source and the grey markers represent hot-pressed samples with carbon black. The SiC-powder has a specific surface area of $13 m^2 g^{-1}$.

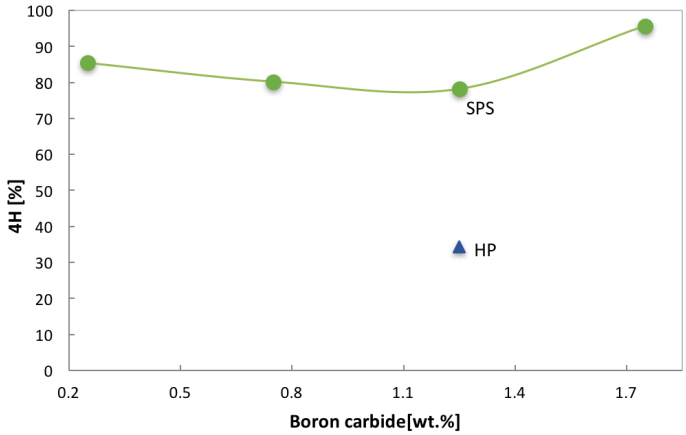


**Figure 4.12:** The amount of 4H measured by Rietveld fitting in Topas. It is assumed that 6H and 4H are the only polytypes present. This illustrates the how the polytypes change with the different amount of boron carbide in spark plasma sintered SiC. The blue triangle is a hot-pressed sample for comparison.

## 4.4 Mechanical properties

### 4.4.1 Hardness measurements

10 measurements were conducted with Vickers micro-indentation on each sample. The average values were plotted together with uncertainty bars based on a standard deviation of the measurements. The values measured are listed in Tab. B.4 and Tab. B.5 in Appendix B. Fig. 4.13 shows the average hardness of the samples with carbon black, but different particle sizes. The samples without binders show

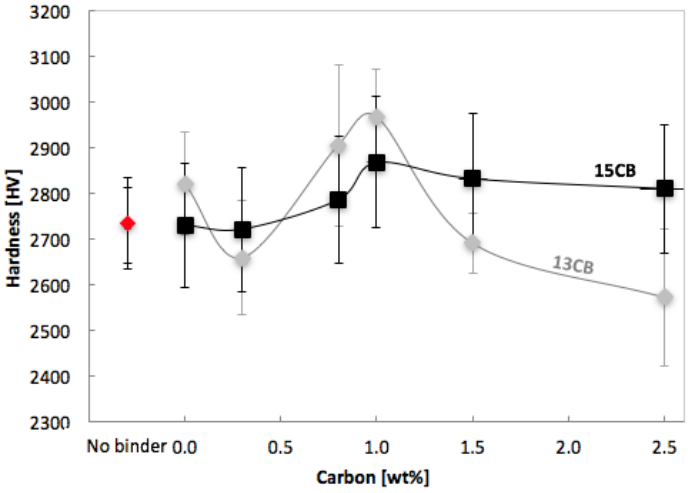


**Figure 4.13:** Measured hardness of hot-pressed samples with carbon black as carbon source, but with different particle surface area 13 $m^2g^{-1}$ (13CB) and 15 $m^2g^{-1}$ (15CB). The red markers represent the samples without binder. The uncertainty bars are based on standard deviation of 10 measurements.

approximately the same hardness for both 13CB and 15CB, with around 2730 HV. The hardness increases with increasing carbon content up to a critical value. The maximum values are with 1.0 wt% C at 2968 HV and 2868 HV for 13CB and 15CB respectively. For 13CB, it is a drastic decline in hardness with a further increase in carbon content. The hardness of 15CB is approximately constant with a further increased carbon content. The influence of carbon source on hardness is further investigated in Fig. 4.14, where the same sized SiC-powder are added resin, 13R, and are plotted together with 13CB.

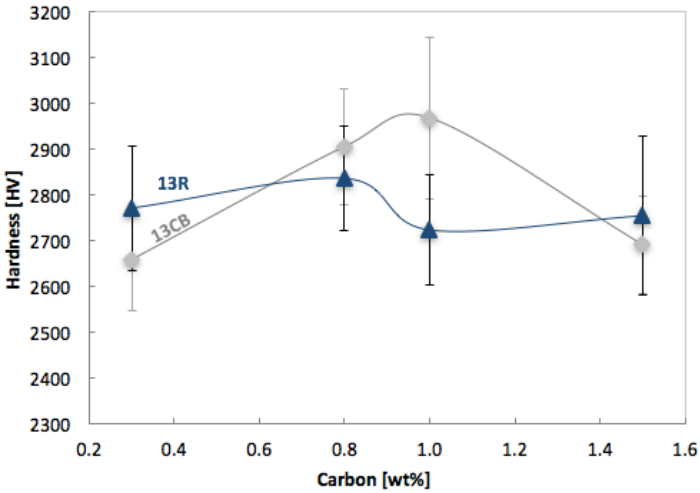


**Figure 4.14:** Measured hardness of hot-pressed samples with same specific surface area 13 $m^2g^{-1}$, but two different sources of carbon: resin (13R) and carbon black (13CB). The uncertainty bars are based on standard deviation of 10 measurements.

The hardness of the samples are more or less equal in the two series, except at 1.0 wt% C, where the hardness of 13CB is almost 300HV higher than 13R. With a focus on the average values only, 13R has a higher hardness than 13CB at 0.3 wt% C with 2800 HV, but there is only a small increase in hardness up to 0.8 wt% C, before the hardness drops again.

The hardness measurements conducted on SPS-samples with a variation in boron carbide content are shown in Fig. 4.15. The first sample with 0.2 wt% $B_4C$ has the lowest measured density with 2640 HV, while 13B0.8 has the highest density with 2923 HV. The average value decreases somewhat with a further increase in boron carbide content, but the middle samples 13B0.7 and 131.2 have large uncertainty bars, which make it difficult establish a trend. Approximately 100 HV distinguish the average hardness of the hot-pressed sample to the sample sintered with SPS. However, the values lie within the uncertainty bars of both samples. Further investigation of the indents was done in a scanning electron microscope (SEM), which confirms the trends presented in the figures. SEM-images of two indents of each sample can be found in Fig. C.3, C.4, C.5 and C.6 in Appendix.

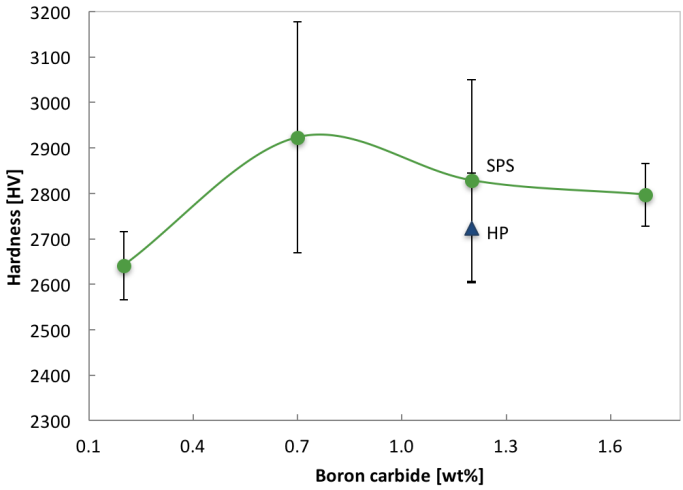


**Figure 4.15:** Measured hardness of spark plasma sintered samples and with a variation of boron carbide, but a constant carbon content. A hot-pressed sample (blue) of same powder is used for comparison. The uncertainty bars are based on standard deviation of 10 measurements.

### 4.4.2 Fracture toughness

The fracture toughness for each sample was calculated from Eq. 3.2 where the indent sizes and crack lengths are based on ten measurements. It is worth mentioning that samples values from Skarpeid [62], 13CB0.3-13CB1.5 and 15CB0.3-15CB1.5, are based on one indent per sample. The calculated fracture toughness of 13CB and 15CB can be seen in Fig. 4.16.

The trend in 13CB is very similar to the trends in density measurements and hardness, with a small decrease from sample 13CB0.8 to 13CB1.0 and a larger decrease down to sample 13CB2.5. For 15CB, the trend is not as clear. There is an increase in fracture toughness up to 15CB0.8 and then a decrease down to 15CB1.0, before it is a small increase up to 15CB2.5, which has the same value as 13CB2.5. The 15CB-series has the highest fracture toughness with no carbon, but the other values are rather low compared to 13CB.

Fig. 4.17 shows how the fracture toughness is influenced when two different carbon sources are used. The uncertainty in the measurements lies within the size of the markers for 13R. The same trend is visible in both series. The fracture

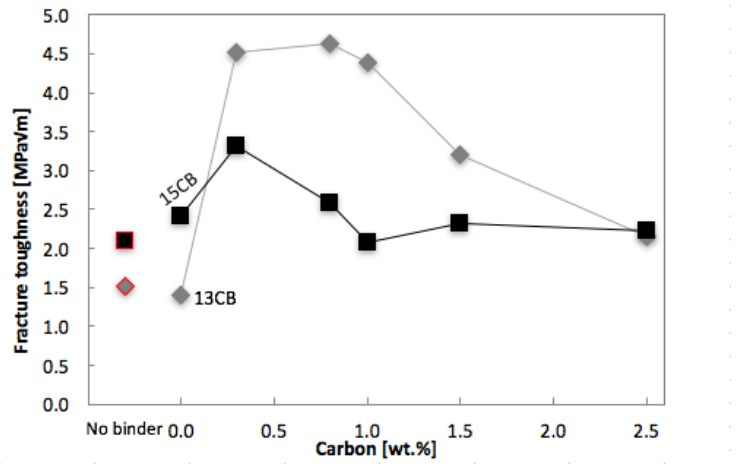


**Figure 4.16:** Measured fracture toughness of hot-pressed samples with carbon black as carbon source, but with different particle surface area 13 $m^2g^{-1}$ (13CB) and 15 $m^2g^{-1}$ (15CB). The red markers represent the samples without binder.

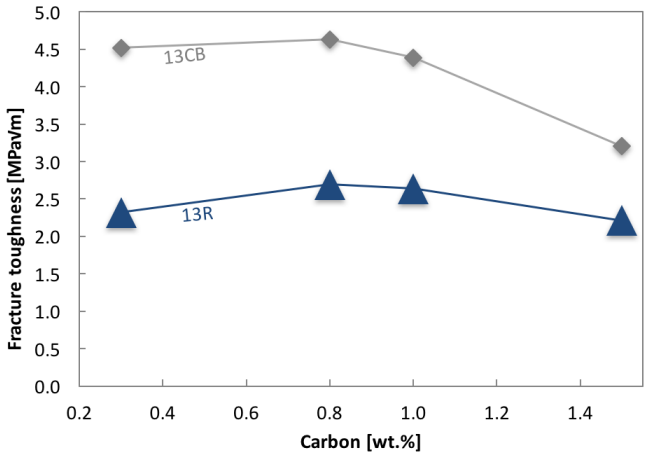


**Figure 4.17:** Measured fracture toughness of hot-pressed samples with equal specific surface area 13 $m^2g^{-1}$, but two different sources of carbon: resin (13R) and carbon black (13CB). The uncertainties of 13R lie within the markers and they are based on the standard deviation of 10 measurements.

toughness increases from 0.3-0.8 wt% carbon before it declines with further carbon addition. However, the values are quite different. The highest fracture toughness is 4.5 MPa$\sqrt{\text{m}}$ for 13CB0.8, but it is only 2.7 MPa$\sqrt{\text{m}}$ for 13R0.8.

Fig. 4.18 shows the calculated fracture toughness of the samples sintered by SPS and a varied boron carbide content. The fracture toughness is more or less constant around 2.1 MPa$\sqrt{\text{m}}$, and independent of the amount of boron carbide. Based on the calculations, it can be seen that the hot-pressed sample has a higher fracture toughness with an average value of 2.6 MPa$\sqrt{\text{m}}$.

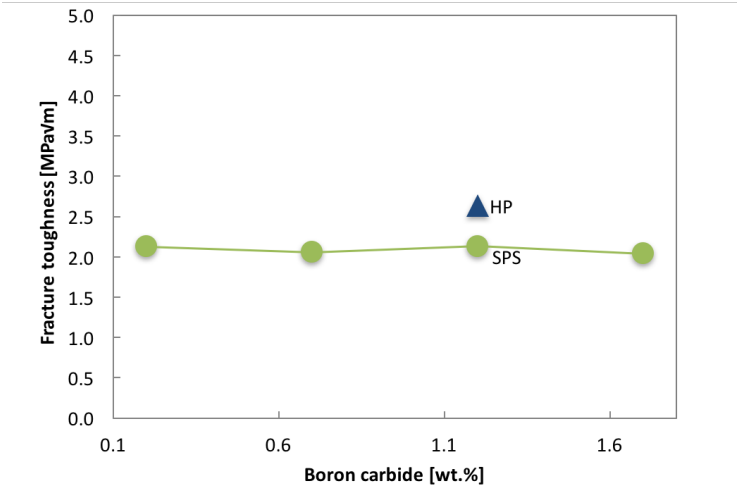


**Figure 4.18:** Measured fracture toughness of spark plasma sintered samples with a variation of boron carbide, but a constant carbon content. A hot-pressed sample (blue) of the same powder is used for comparison. The uncertainties lie within the markers and they are based on the standard deviation of 10 measurements.

### 4.4.3 Failure analysis

Scanning electron microscopy(SEM) images of the fracture surfaces can be found in Fig. 4.19. Examination of the samples without binder, Fig. 4.19a and Fig. 4.19c, show rather smooth surfaces, which indicate a high degree of transgranular fractures. There are also some larger grains present. This is also seen in the samples with binder but without carbon in Fig. 4.19b and Fig. 4.19d. Here, it is also very easy to see the outline of the many smaller grains between the larger ones. In

all the samples without carbon, there are rather many small, black circles on the images, which most likely are pores. These are also located within the grains on the images. The samples with 2.5 wt% carbon black can be seen in Fig.4.19e and 4.19f. The fracture surfaces show a lot of topography and it is not possible to distinguish between grains. These samples have therefore a much larger degree of intergranular fractures. The fracture surface also revealed some black areas in the samples, which can be seen in Fig. C.1 in Appendix. It is uncertain whether this is carbon or pores, or a mixture, but it will in all cases lead to a weaker material.

The samples in these series with carbon content from 0.3-1.5 wt% show a mixture between both fracture modes, but sample 13CB1.5 shows more intergranular fracture surface than the rest. The fracture surfaces of the samples with carbon content from 0.3-1.5 wt% taken by Skarpeid[62], can be found in Fig. C.2 in Appendix C.

Fracture surfaces of the samples with resin as carbon source are shown in Fig. 4.20. The images are quite similar to the correlating images of the samples with carbon black and same particle size. With 0.3 wt% carbon, there is most transgranular fractures, but there a higher degree of intergranular fractures with increasing carbon content.

Fig. 4.21 shows the fracture surfaces of the samples with variation in boron carbide content and a constant amount of carbon (1.0 wt%). The fracture surfaces look similar independent of boron carbide content, with a mixture of intergranular and transgranular fractures. There are larger anisotropic grains present in all the images.

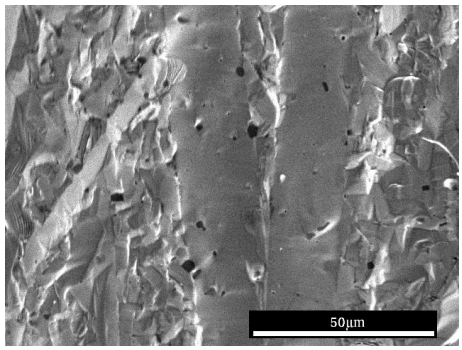


**(a)** F13CB00

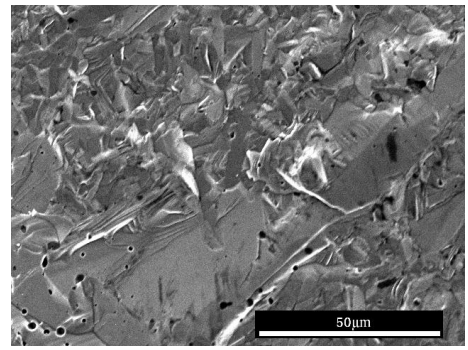


**(b)** 13CB0

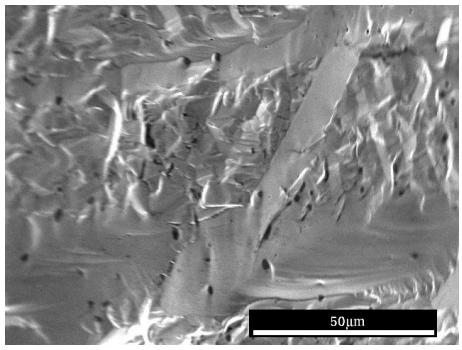


**(c)** 15CB00

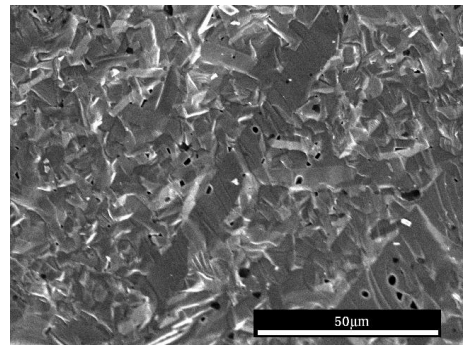


**(d)** 15CB0

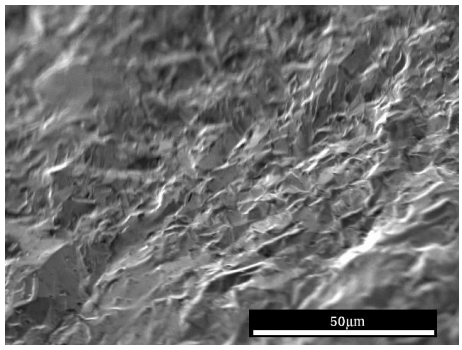


**(e)** 13CB2.5

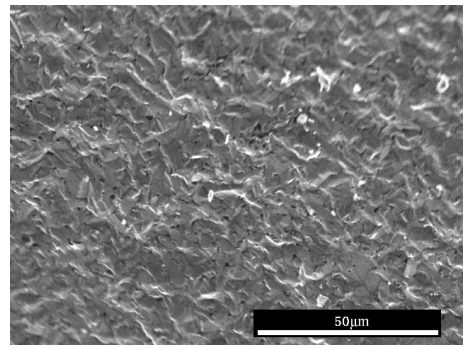


**(f)** 15CB2.5

**Figure 4.19:** SEM images of fracture surfaces of the hot-pressed samples with different amount of carbon black and two different surface area of the SiC-powder: 13 $m^2g^{-1}$ (13CB) and 15 $m^2g^{-1}$ (15CB).

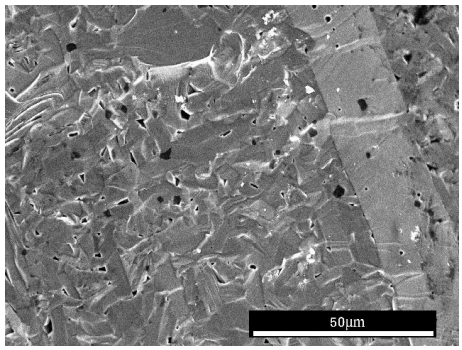


**(a)** F13R0.3

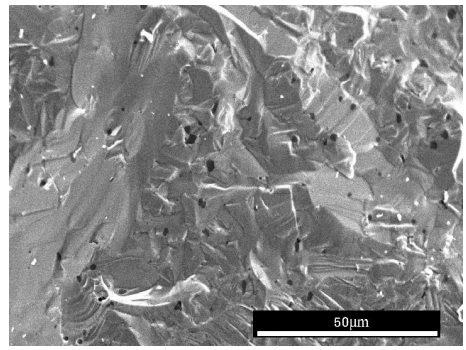


**(b)** F13R0.8

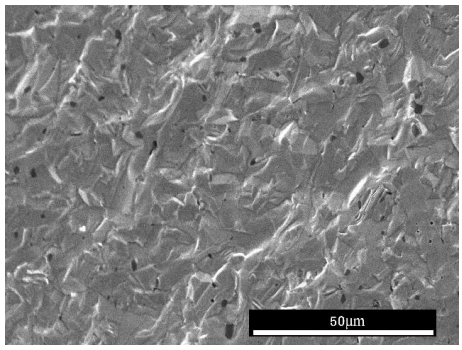


**(c)** F13R1.0

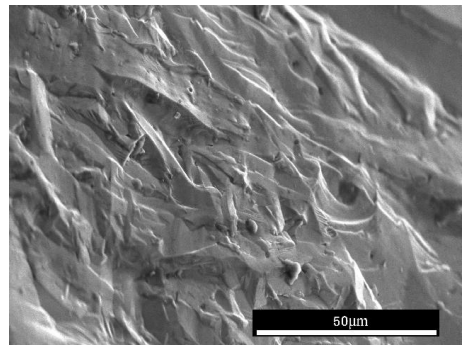


**(d)** F13R1.5

**Figure 4.20:** SEM images of fracture surfaces of hot-pressed samples with variation in carbon content and resin as carbon source. The SiC-powder has a specific surface area of 13 $m^2g^{-1}$.

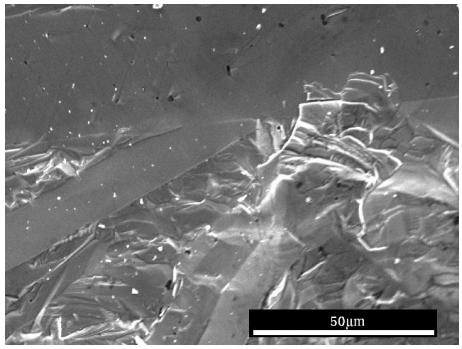


**(a)** F13B0.2

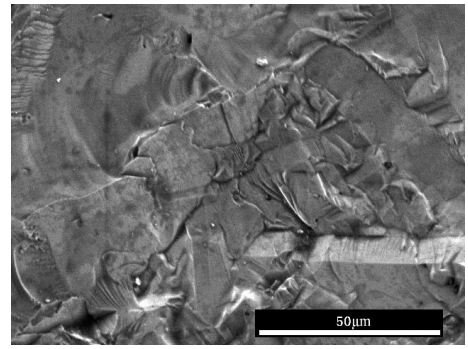


**(b)** F13B0.7

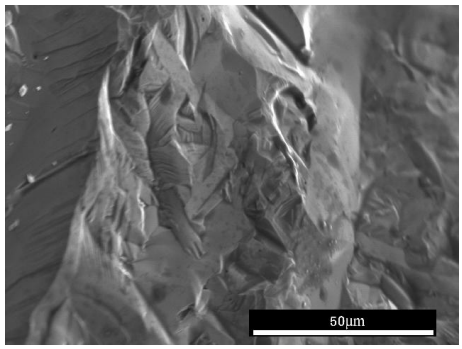


**(c)** F13B1.2

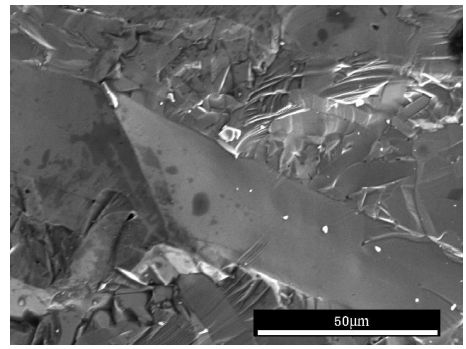


**(d)** F13B1.7

**Figure 4.21:** SEM images of fracture surfaces for the spark plasma sintered samples with a variation in boron carbide content and a constant amount of carbon. The SiC-powder has a specific surface area of 13 $m^2g^{-1}$.

# Chapter 5

# Discussion

This chapter will discuss the results presented in the previous chapter. The sections will be presented in the same order, starting with microstructure and density measurements, before phase composition will be discussed. Lastly, the mechanical properties will be analysed. The samples will be presented in the same order, first the two cases with a varying carbon content with a focus on particle sizes and carbon source. Then, samples with variation boron carbide content will be discussed.

## 5.1 Microstructures

The SEM-images of etched surfaces showed a rod-shaped grain morphology. The applied pressure during sintering will result in flat grains in the pressing direction, as mentioned in Section 2.3.2. Increased grain growth will, therefore, result in elongated grains as the preferred growth direction is normal to the pressing direction. Some of the grains will be oriented in that direction and have a much higher driving force for grain growth and that explains why some grains are much larger than others. The grain growth takes place in the final sintering stage. All the samples have been produced in the same way, so it can not be caused by different dwelling time during sintering. The particle size distributions of powders have not been analysed, and could have some influence on the grain morphology of the sintered samples.

The images show a decrease in grain growth with increasing carbon content. The number of anisotropic grains did also decrease somewhat with increasing carbon content. With higher carbon content (2.5 wt.%) there were some elongated grains, but a higher ratio of spherical grains than obtained with no carbon addition. This indicates that carbon is a grain growth inhibitor. This is also seen in other experiments.[51;6;8] There were less anisotropic grains present in 15CB compared to 13CB. This can be due to less of the polytype 4H in the powder prior to sintering, as 4H most likely are the large, anisotropic grains seen in the sintered samples.

The samples with resin showed less of these large abnormal grains for the samples with low carbon content. This is mostly like due to a more homogeneous distribution of carbon as resin is added as liquid, which is more accessible for all SiC-grains and carbon acts as a grain growth inhibitor. The overall large grains in 13R1.5 is probably caused by extensive grain growth due to higher sintering temperature as the pyrometer was broken.

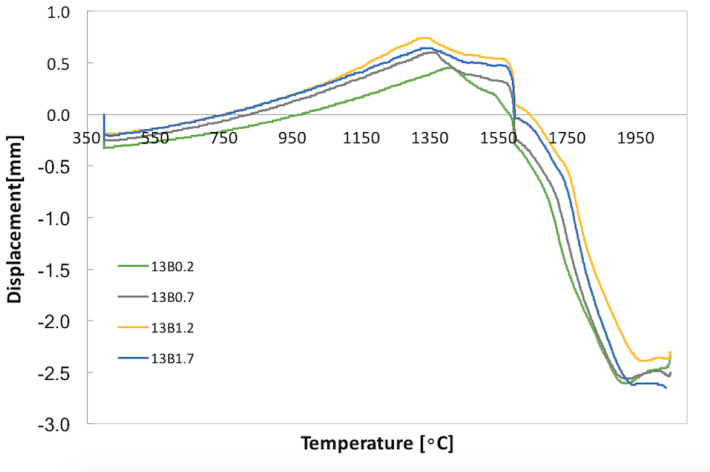


**Figure 5.1:** Displacement of the samples during spark plasma sintering. This is measured along the z-axis and a negative slope means a decrease in the sample height, i.e. shrinkage.

All the samples sintered with the SPS show a lot of grain growth. To avoid grain growth, the sintering temperature and holding time should have been decreased. The sintering program measures the displacement of the samples along the z-axis, and this is plotted in Fig. 3.4. From the figure, it is possible to see that the sinter-

ing starts around 1600 °C, which is conclusive with sintering equations presented earlier. The samples stop shrinking at 1950 °C, which means that most of the densification are finished. This is not an exact measuring method, but show that a lower sintering temperature should be sufficient for densification, which would give less grain growth. It is also worth mentioning that the pressure used was 20 MPa, but other sources found use pressure from 40-100 MPa.[59;65]

13B0.2 showed less grain growth than the other sps-samples. One explanation can be that the low boron content decreases the rate of densifying mechanisms which boron contributes to. With a decreased rate, densification takes longer time, leading to less time for grain growth in the final sintering stage. 0.2 wt% $B_4C$ are possibly lower or on the solubility limit of boron in SiC, so the rate of densification will increase when more boron is added. The rest of the spark plasma sintered samples have approximately the same grain growth, which means that the amount of boron carbide added is sufficient and there is no need to exceed 0.7 wt% $B_4C$.

## 5.2 Density measurements

The densities measured by Archimedes' method should show lower values than the densities measured with helium pycnometer, as the helium pycnometer does not measure open porosity. The open porosities measured are very low, which is consistent with sintering theories. All samples had density >92 %, so the intermediate sintering stage is completed and all the porosity should, more or less, be closed porosity. Based on three measurements of four samples, both methods showed a low and similar uncertainty in the measurements.

As discussed in the theory, carbon removes $SiO_2$ from the particle surface. When a surplus of carbon is added, the excess carbon will be trapped at grain boundaries and the bulk density will slightly decrease. This may be the case for the samples with 2.5 wt% carbon, where the density is similar, even with an unequal specific surface area. Fracture images in Fig. C.1 show defect areas with a higher concentration of carbon and/or pores. EDS analysis showed a much higher concentration of carbon, but pores can not be excluded either. It is also worth mentioning that the relative densities would be increased if the carbon content had been included in the theoretical density, but the amount of excess carbon is unknown and they have the highest closed porosity.

For the samples with 1.5 wt% C, 13CB1.5 had a decrease in density, while 15CB1.5 the same density as the samples with less carbon. This can be explained by a higher surface area for 15CB, which will require more carbon to remove the silica layer. Hence, less excess carbon present.

The samples without carbon achieved densities >98 %, which is higher density than found in literature (94 %)[6]. Samples without binder (PVA) were tested to exclude binder as a carbon source. The density decreased with around 0.5 %, which indicate that the binders do contribute somewhat to increased density. It is hard to say if the density difference is caused by carbon residuals from binder, or that the binder increases the flow properties so that density gradients are minimised. However, the densities are still very high. One explanation may be that there is some free carbon in the SiC-powder (max 0.25 %), which may contribute to the sintering process. Otherwise, hot-pressing is an effective sintering method, which reduces the amount of sintering additives needed. It might be that carbon addition is not essential for obtaining high densities in pressure sintering, and that $SiO_2$ is reduced by itself by the proposed reaction in Eq. 2.5. Based on the densities found, Sample 13CB0.8 and 15CB1.0 have the highest density. Hence, the optimum carbon content with respect to density is 0.8 wt% and 1.0 wt% for 13CB and 15CB, respectively. For comparison, Stobierski et. al[6] hot-pressed SiC-powder with a surface area of 15 $m^2g^{-1}$ and had a maximum density with 1.5 wt% carbon.

It was expected, based on literature, that the samples with resin as carbon source should have higher densities, especially at lower concentration of carbon. This is because resin is a liquid, which increases the possibility for a homogeneous distribution. However, based on these measurements, the samples with resin have lower densities or the same densities, depending on the method used. The measuring chamber in the helium pycnometer used for these samples, differ. Hence, larger uncertainty for 13CB and the open porosity is not measured, so it is therefore expected that the trends from Archimedes' method (Fig.4.5b) are the most representative. The reason behind so similar densities can be that carbon black is well distributed due to proper mixing of the slurry prior to spray-drying. It is also possible that the samples with resin contain less carbon than assumed as the decomposition of resin have not been tested on the powders. Other ideas can be that the differences in densities will be larger if lower carbon contents had been tested.

Fig 4.7 show the density measurements conducted on samples with different boron carbide content and a constant amount of resin. Based on these results, the highest density is achieved with 0.2 wt% $B_4C$. The content is close to the calculated solubility limit in SiC, and lower than the optimised content from other sources, which has been 0.3 wt%[8] and 0.2-0.5 wt%[57]. The trend seen is otherwise consistent with literature, with a decrease in density with a further addition of boron carbide.[54] The hot-pressed sample shows a density that is 1 % higher than the density obtained by SPS. This might have been because the SPS program is not optimised, as explained previously, and there is a lot of exaggerated grain growth. When the grains grow too fast, pores can be trapped within the grains so they are impossible to remove and the density decreases. A related point to consider is that these samples are sintered with SPS, which is a very effective sintering method. The reference values are based on hot-pressed samples. More samples should have been sintered with both SPS and hot-press, with a better SPS program, in order to give a complete theory.

### 5.2.1 Phase composition

There are several possible origins of the graphite phase found by X-ray diffraction. The first one is impurities present in the starting powders of SiC or $B_4C$ prior to sintering. This can be present as there is a small amount of free C in SiC powder due to the graphitisation that happens in the inner part of the core in the Acheson furnace and because of free carbon from raw $B_4C$, which can graphitise.[66] However, these impurities would have been present in all the samples, which does not explain the intensity variations in the samples. The most likely origin of the intergranular C-phases is graphitisation of the carbon additives during densification. Graphitisation happens in the region 1000-3000 °C for carbon blacks.[67] Different materials that act as carbon sources undergo the same graphitisation process.[68] Resin acts as both binder and carbon source for sample 13R and 13B. However, the amount of carbon left after decomposition can be discussed. Three possible reactions are proposed for decomposition of Resol Resins in reducing atmosphere, and the theoretical amount of carbon left varies from 48-66 wt%.

$$C_{13}H_{12}O_2 \rightarrow 2CO + 3CH_4 + 8C \tag{5.1}$$

$$C_{13}H_{12}O_2 \rightarrow 2H_2O + 2CH_4 + 11C \tag{5.2}$$

$$C_{13}H_{12}O_2 \rightarrow CO + H_2O + 2.5CH_4 + 9.5C \tag{5.3}$$

In addition, it has been seen that the rate of graphitisation is faster for boronated carbons, for instance when the rate increased by 10 when 0.5 wt% B was added, and the graphitisation of amorphous carbon starts 400-500 °C lower than carbons containing no boron. However, the mechanisms are a bit unclear, but the activation energy was independent of boron concentration.[69]

The XRD-diagrams in Fig 4.8 shows that the diffraction line of graphite increases with increasing carbon content. In the 13CB-samples, the peak is visible at 0.8 wt% carbon, but it is not clearly visible until 1.5 wt% carbon for 15CB. This indicates that more than 1.0 wt% carbon is needed to react with silica in the 15CB-samples, compared to 0.8 wt% carbon in the 13CB-samples. The difference is most likely due to different surface area, and smaller particles need more carbon to remove silica at the particle surface.

In the samples with resin, there is less graphite present than in the samples with carbon black. This might be explained by less carbon transformed into graphite, due to the different chemical compositions of the carbon sources, so that the excess carbon is present as an amorphous phase at the grain boundaries, which will not be detected with XRD. It is also possible that the samples with resin contain less carbon than expected, which varies according to the equation given above. On the other hand, the diffraction line for graphite is noticeable for both 13CB and 13R with 0.8 wt%, which means that there is some graphite present. It is therefore unlikely that there is a large difference in the amount of carbon in the samples.

From the XRD-diagrams of the samples with different boron carbide, shown in Fig 4.9, it is possible to detect the graphite in all samples. The diffraction line intensity of 13B1.2 coincides with 13R1.0, which was expected as the samples are from the same powder. Unanticipated, the intensity of the carbon peak increases as the boron carbide content increases, especially 13B1.7 stands out. This may confirm the theory stated above, that boron influences the graphitisation, as the intensity of the graphite peak is very low for 0.2 wt% $B_4C$. The larger amount of B in 13B1.7 might enhance the graphitisation process of amorphous carbon, resulting

in more graphite in the sample. Another theory to consider is that there might be more carbon at the grain boundaries when the boron carbide concentration is enhanced. Boron diffusivity in SiC is high, and there is no difference if B or $B_4C$ is added. So if boron substitutes for Si or C in the lattice, which explained earlier will create vacancies and lower the activation energy for diffusion and thereby increase sintering, there will be an increased concentration of carbon at the grain boundaries. B is most likely to substitute C and form $SiB_4$, due to similar lattice parameter.[16] It is therefore possible that the high amount of boron carbide result in a carbon depletion in the SiC structure, and increase the total amount of carbon at the grain boundaries illustrated with the following equation:

$$B_4C(s) + SiC(s) \rightarrow SiB_4(s) + 2C(s) \tag{5.4}$$

Phase diagram of boron carbide has a graphite phase present at 20.6 at%C and above.[70;66]

It is not possible to detect any boron carbide phase, most likely due to low concentration and the fact that it is soluble in SiC. In addition, the boron carbide phase (PDF 01-086-1120) has its major peaks at 35° and 38° which overlaps with diffractogram lines for SiC.

The XRD-diagrams also show different amount of the polytypes present. The 2H phase could not be ruled out as it has overlapping peaks with other phases. However, it is very unlikely that 2H is present as it is a more uncommon polytype, which is thermodynamic stable below 1600 °C.[13] It seems that it is valid assumption that 6H and 4H are the only polytypes present. Both polytypes, 4H and 6H, are thermodynamically stable at the sintering temperature.[13]

The formation of 4H can be explained by the addition of boron. However, the amount of boron added is similar for all the samples where carbon is the only changed factor and does not explain the observed differences in ratio between the samples, as seen in Fig. 4.10. This may be explained by the difference in the specific surface area as the transformation also involves surface diffusion mechanisms, but the difference in surface area is rather small.[15] Non-sintered powders show that there is a difference in 4H content prior to sintering as well. The content in 13CB0.3 was over four times higher than the content in 15CB0.3. The measurements show that the number of 4H-phases increases with sintering.

When comparing the microstructures with the presence of the different phases,

it seems like all the samples with much exaggerated grain growth contain the most 4H. Especially the SPS-samples and 13R1.5, which was exposed to higher sintering temperature. One theory is that the 4H-grains grow more rapidly than 6H, so 6H grains are consumed by larger 4H grains. This is consistent with theory presented, where elongated grains were formed by the presence of 4H, and 4H grains grow rapid with increased temperatures.[17;18] This will also explain the reason why the SPS-sample had so much more 4H than the hot-pressed sample. The basis composition of the powder was the same, but high sintering temperature made it possible for the 4H grains to grow more rapidly.

There is a significant reduction of 4H for 13CB and 13R with increasing carbon content. However, it is less pronounced for 15CB. The amount of phases found have some uncertainty due to texture. However, this can not explain the larger differences between the samples. It might be because carbon limits grain growth, and thereby inhibits some of the abnormal 4H grain growth, which will decrease the total amount of 4H.

## 5.3 Mechanical properties

### 5.3.1 Hardness

The trend obtained from the hardness measurements is relatively similar to the density trend measured for the samples with carbon black, 13CB and 15CB. Sample 13CB1.5 shows a relatively low hardness compared to 13CB1.0. The excess carbon has formed a secondary graphite phase (as seen in the XRD-diagram), which will increase grain boundary sliding, making the material weaker. The same trend is not detected for 15CB, which can be because of larger surface area. Hence, more carbon is needed to remove the silica as explained earlier. Larger black areas of either carbon or pores were found in 13CB2.5 both at the etched surface and inside the sample, normal to the pressing direction. These areas will anyhow be a flaw in the material with high probability for failure. The samples with increased amount of needle-like grains will have internal anisotropy, which increase the stresses in the material. This will decrease the hardness, but increase the fracture toughness due to toughening mechanisms. This may explain the behaviour of 13CB0.3 (and the other samples with low carbon content), as the sample had many thin, needle-

shaped grains.

When comparing the samples with different carbon sources it is possible to see that the hardness is relatively similar and the values lie within the uncertainty bars. This can be linked to relative equal microstructures and densities, which already have been discussed. Then again, with a focus on the average values only, 13R has higher hardness with 0.3 wt%, but a relative lower hardness at 1.0 wt%. This can be explained by a better distribution of carbon with resin, which increases the overall sintering at low concentrations and increases the grain boundary strength. The decrease in hardness happens when excess carbon are located at the grain boundaries, which increase the possibility for grain boundary sliding. However, increased density for 13R0.3 compared to 13CB0.3 was not detected by density measurements.

The hardness trend for the samples with variation in boron carbide content is different from the density trends. 13B0.2 had the highest density, but the lowest hardness. This might be due to smaller grains. Sample 13B0.2 had smaller grains and hence, more grain boundaries. The probability of measuring the hardness at grain boundaries will therefore increase, which will decrease the average hardness as well. The other samples had larger grains, which gave a high hardness (>2800 HV). The hot-pressed sample had lower hardness, but also smaller grain than the SPS-sample. The other samples show a very small decline in hardness with increasing boron carbide content, which can be explained by reduced density as the excess $B_4C$ segregates SiC and a secondary phase at the grain boundaries will often weaken the material, even though $B_4C$ is a hard material itself.

The average hardness values measured are higher than most literature values for SiC, and the indent images taken in SEM showed a minor decrease in indent size compared to the one measured with Vickers micro-indentaion, which gives an even higher hardness. However, the uncertainty bars are large. The indent sizes studied in SEM varied a lot, which confirms the large uncertainty bars in the hardness measurements. The measured hardness of a material will depend on whether the diamond hits the grain or the grain boundary. The grain boundary has lower hardness, and will also influence the values obtained. The measurement variations can also be a consequence of different crystallographic directions of the silicon carbide grains since the various directions have different hardness. [23]

### 5.3.2 Fracture toughness

The samples showed a reduced grain size with increasing carbon content, and a reduced grain size will normally give a higher fracture toughness. However, there are large acicular grains present in the samples, that can increase the fracture toughness by crack deflection, pullout and crack bridging. The presence of these toughness mechanisms explains the relatively high value for 13CB0.3, 13CB0.8, 13CB1.0 and 15CBB0.3. Samples with 1.5 %C and 2.5 %C had very few or none of these larger grains, which can explain the decrease in fracture toughness, even though the grains were smaller. 13CB2.5 had also the highest amount of excess carbon present, as seen in Fig. 4.8. The carbon will form a secondary graphite phase on the grain boundaries, which will weaken the material. The 15CB-samples had smaller and a less amount of acicular grains and that might be the reason why the fracture toughness measured are lower.

There is a relatively large difference in the calculated fracture toughness between the samples with carbon black and resin. Even tough the values of 13CB-series are only based on one indent per sample, the uncertainty in the 13R-samples are not close to the values obtained with 13CB, and it is therefore possible to conclude that the samples with carbon black have higher fracture toughness. Based on the images of the microstructures, the samples with resin have less of these large needle-grains, which will decrease the toughness. Polishing was improved on these samples, compared to the samples from the specialisation project. Many scratches in the samples may have camouflaged cracks so they were not to detected, which in turn leads to improperly increased fracture toughness.

The calculated fracture toughness was independent of the boron carbide content. This can be seen in conjunction with a rather similar microstructure for all the samples. The samples had large grains due to grain growth during sintering, which explain the lower toughness compared to the hot-pressed samples.

The 13CB-samples have most of the values above literature values, while the rest of the samples are in the lower range of reported values.[32] However, the fracture toughness is very dependent on the method used and it can therefore be tricky to compare values. Most of the measurements correlate with literature values found, but the methods deviate from the one used in this work. The constant used in the formula for fracture toughness has an uncertainty of $\pm$ 0.004.[65] This may result in

up to a 24% increase in fracture toughness.

### 5.3.3 Failure analysis

All the samples show a mixture between intergranular and transgranular fractures. However, the degree of intergranular fracture for 13CB1.5 13CB2.5 and 15CB2.5, i.e. the samples with the most carbon, are much larger than the rest of the samples. This can also be explained by the formation of a graphite phase at the grain boundaries during sintering. This will weaken the grain boundaries and thereby increase the rate of intergranular fracture. These results also confirm the theory stated earlier, that the samples with larger surface area, 15CB, consume more carbon so that less graphite is present at the grain boundaries and thereby transgranular fractures dominate. In the samples with varied boron carbide content, the grain sizes are very large, which gives a fracture surface with little topography.

# Chapter 6

# Conclusion

Three different commercial SiC-powders Denitec 13H (13CB), Densitec 15H (15CB) and Densitec 13HR (13R) were hot-pressed with different amount of carbon, ranging from 0-2.5 wt%. Densitec 13HR with various amount of boron carbide (0.2-1.7 wt%) and 1.0 wt% C were sintered with spark plasma sintering.

The samples were characterised according to density, mechanical properties, microstructure and phase composition and the main findings are summarised as follows.

- Densitec 15H, with a higher specific surface area, consumes more carbon during sintering than Densitec 13H. The excess carbon forms a secondary graphite phase at the grain boundaries, which reduced the density and hardness and gave more intergranular fractures in both samples.
- High density (>98.5 %) and hardness (>2750 HV) were obtained even without carbon addition.
- Carbon limits grain growth during sintering.
- The density, hardness and fracture mode are approximately equal regardless if resin or carbon black is used as carbon source. The sample with carbon black (13CB) had more of large needle-shaped grains, which increased the fracture toughness.
- 0.2 wt% $B_4C$ gave the highest density, but lowest hardness. The optimised

boron carbide content based on density and mechanical properties are therefore 0.7 wt%, which is lower than the concentration used today (1.2 wt%)

- The spark plasma sintered samples had considerable grain growth during sintering. The large grains affected the mechanical properties and resulted in high hardness, but low fracture toughness.
- All samples with a significant amount of large anisotropic grains had more of the polytype 4H. Based on this observation, it is possible to say that the anisotropc grains consist of polytype 4H and the amount of 4H is high due to rapid growth at the sintering temperature.

All values obtained are rather high, but these results are based on only one sample with a given geometry. In order to improve the validation of the results, there should be done at least one additional testing with the same powders to investigate the reproducibility.

# Chapter 7

# Further work

Based on the measurements done, no or very little carbon and boron carbide are necessary to obtain high density for pressure sintering. It would be very interesting to sinter a sample without any boron carbide and see if high density is obtainable even without any additives. Additional testing of boron carbide in the range of 0-0.7 wt% should be done to get a more optimised concentration.

One of the questions still debated in literature is how boron aid in densification. In order to understand more of which mechanisms boron contributes to, there should be more examination of the bulk SiC grains and grain boundaries with analysis method where it is possible to detect elements with this low concentration. One suggestion is to try atomic probe tomography (APT), which has the highest spatial resolution of any microscopy technique.[71] It is beneficial to know which mechanisms the additives contribute to in order to optimise the concentration of additives and tailor the mechanical properties.

# Bibliography


[1] D. Richerson, *Modern Ceramic Engineering: Properties, Processing, and Use in Design*. New York, USA: Taylor & Francis Group, 3th edition ed., 2006.

[2] B. Matovic and T. Yano, "Silicon Carbide and Other Carbides: From Stars to the Advanced Ceramics," *Handbook of Advanced Ceramics:Materials, Applications, Processing, and Properties. Academic Press: Elsevier Inc.*, pp. 225–244, 2013.

[3] C. H. Foundation, "Edward Goodrich Acheson." `https://www.chemheritage.org/historical-profile/edward-goodrich-acheson`, 2015. [Online; accessed 15-september-2016].

[4] Saint-Gobain, "SAINT-GOBAIN SILICON CARBIDE." `http://www.sic.saint-gobain.com`, 2016. [Online; accessed 18-January-2017].

[5] M. Rahaman, *Ceramic Processing and Sintering*. New York, USA: Marckel Dekker,Inc., 1995.

[6] L. Stobierski and A. Gubernat, "Sintering of silicon carbide I. Effect of carbon," *Ceramics International*, vol. 29, no. 3, pp. 287 – 292, 2003.

[7] E. Gross, B. Dahan, and W. Kaplan, "The role of carbon and $SiO_2$ in solid-state sintering of SiC ," *Journal of the European Ceramic Society*, vol. 35, no. 7, pp. 2001 – 2005, 2015.

[8] Y. Murata and R. Smoak, "Densification of Silicon Carbide by the Addition of BN,BP and B4C, and Correlation to Their Solid Solubilities.," *The International Symposium of Factors in Densification and Sintering of Oxide and NON-oxide Ceramics*, pp. 382–392, 1978.

[9] G. Gupta, P. Kumar, V. Rudolph, and M. Gupta, "Heat-transfer model for the acheson process," *Metallurgical and Materials Transactions A*, vol. 32, no. 6, pp. 1301–1308, 2001.

[10] A. Qteish, V. Heine, and R. Needs, "Structural and electronic properties of sic polytypes," *Physica B: Condensed Matter*, vol. 185, no. 1, pp. 366 – 378, 1993.

[11] NSM Archive- Physical Properties of Semiconductors, "SiC-Silicon Carbide." `http://www.ioffe.ru/SVA/NSM/Semicond/SiC/basic.html`, 2016. [Online; accessed 29-september-2016].

[12] G. Harris, *Properties of Silicon Carbide*. London, United Kingdom: INSPEC The institution of Electrical Engineers, 1995.

[13] N. Jepps and T. Page, "Polytropic Tranformation in Silicon Carbide," *The Ceramics Group,Department of Metallurgy and Materials Science, University of Cambridge,Pembroke Street, Cambridge, U.K.*, pp. 259–307, 1982.

[14] Y. Inomata, Z. Inoue, M. Mitomo, H. H. Suzuki, and Yogyo-Kyokai-Shi, "Relation between growth temperature and the structure of SiC crystals grown by the sublimation method," *Emmanuel Coll Boston mass oriental science research library*, vol. 76, pp. 313–319., 1968.

[15] P. Kistler-De Coppi and W. Richarz, "Phase transformation and grain growth in silicon carbide powders," *International Journal of High Technology Ceramics*, vol. 2, no. 2, pp. 99 – 113, 1986.

[16] M. S. Datta, A. K. Bandyopadhyay, and B. Chaudhuri, "Sintering of nano crystalline $\alpha$ silicon carbide by doping with boron carbide," *Bulletin of Materials Science*, vol. 25, no. 3, pp. 181–189, 2002.

[17] Y. Lee, Y. Park, E. Lee, D. Seo, and Y. Hwang, "Effect of starting phase on microstructure and fracture toughness of hot-pressed silicon carbide," *Materials Letters*, vol. 57, no. 1, pp. 203 – 208, 2002.

[18] H. N. Yoshimura, A. C. Da Cruz, Y. Zhou, and H. Tanaka, "Sintering of 6H($\alpha$)-SiC and 3C($\beta$)-SiC powders with B4C and C additives," *Journal of Materials Science*, vol. 37, no. 8, pp. 1541–1546, 2002.

[19] M. Kanzaki, "Crystal structure data for VESTA ." `http://www.misasa.okayama-u.ac.jp/~masami/pukiwiki/index.php?Vesta_data`, 2016. [Online; accessed 10-October-2016].

[20] SINTEF, "SunSic âĂŞ Efficient Exploitation of the Sun with Intermediate Band Silicon Carbide." `https://www.sintef.no/en/projects/sunsic-efficient-exploitation-of-the-sun-with-inte/`, 2015. [Online; accessed 4-June-2017].

[21] K. Yamada and M. Mohir, *Properties and Applications of Silicon Carbide Ceramics.*, pp. 13–45. London, England: ELSEVIER SCIENCE PUBLISHERS LTD, 1992.

[22] R. W. Rice, C. Wu, and F. Boichelt, "Hardness-grain-size relations in ceramics," *Journal of the American Ceramic Society*, vol. 77, no. 10, pp. 2539–2553, 1994.

[23] P. Shaffer, "Effect of crystal orientation on hardness of silicon carbide," *Journal of the American Ceramic Society*, vol. 47, pp. 466–466, 9 1964.

[24] G. R. Sawyer, P. M. Sargent, and T. F. Page, "Microhardness anisotropy of silicon carbide," *Journal of Materials Science*, vol. 15, no. 4, pp. 1001–1013, 1980.

[25] K. Mogstad, "A study on commercial SiC-powders sintered by hot pressing," Master's thesis, Norwegian University of Science and Technology (NTNU), Norway, 2016.

[26] P. Sargent and T. Page, "The influence of microstructure on the microhardness of ceramic materials.," *Proceedings of the British Ceramic Society*, vol. 26, pp. 209–224., 1978.

[27] R. W. Armstrong, E. L. Raymond, and R. R. Vandervoort, "Anomalous increase in hardness with increase in grain size of beryllia," *Journal of the American Ceramic Society*, vol. 53, pp. 529–530, 9 1970.

[28] T. Tani, Y. Miyamoto, M. Koizumi, and M. Shimada, "Grain size dependences of vickers microhardness and fracture toughness in Al2O3 and Y2O3 ceramics," *Ceramics International*, vol. 12, no. 1, pp. 33 – 37, 1986.

[29] H. Kurishita, H. Yoshinaga, and Y. Ikuhara, *Grain Boundary and High-Temperature Strength in SiC.*, pp. 13–45. London, England: ELSEVIER SCIENCE PUBLISHERS LTD, 1992.

[30] J. Wachtman, W. Cannon, and M. Matthewson, *Mechanical Properties of Ceramics*. New York, USA: John Wiley and Sons, INC., 2009.

[31] Z. Li, A. Ghosh, A. S. Kobayashi, and R. Bradt, "Indentation fracture toughness of sintered silicon carbide in the palmqvist crack regime," *Journal of the American Ceramic Society*, vol. 72, pp. 904–911, 6 1989.

[32] R. Munro, "Material Properties of sintered 6H-SiC.," *American Institute of Physic and American Chemistry Society*, vol. 5, no. 26, pp. 1195–1203, 1997.

[33] Y. Kim, M. Mitomo, and H. Hirotsuru, "Grain Growth and Fracture Toughness of Fine-Grained Silicon Carbide Ceramics," *Journal of the American Ceramic Society*, vol. 78, pp. 3145–3148, 11 1995.

[34] I. McColm and N. Clark, *Forming, Shaping and Working of High-Performance Ceramics*. New York, USA: Blackie and Son, 1988.

[35] M. Rahaman, *Sintering of Ceramics*. New York, USA: Taylor & Francis Group, 2008.

[36] S. Diouf and A. Molinari, "Densification mechanisms in spark plasma sintering: Effect of particle size and pressure," *Powder Technology*, vol. 221, pp. 220 – 227, 2012. Selected papers from 2010 {AIChE} Annual Meeting.

[37] U. Anselmi-Tamburini, J. Garay, Z. Munir, A. Tacca, F. Maglia, G. Chiodelli, and G. Spinolo, "Spark plasma sintering and characterization of bulk nanostructured fully stabilized zirconia: Part ii. characterization studies," *Journal of Materials Research*, vol. 19, no. 11, p. 3263âĂŞ3269, 2004.

[38] Z. Zhaohui, W. Fuchi, W. Lin, L. Shukui, and S. Osamu, "Sintering mechanism of large-scale ultrafine-grained copper prepared by {SPS} method," *Materials Letters*, vol. 62, no. 24, pp. 3987 – 3990, 2008.

[39] Z. Zhang, Z. Liu, J. Lu, X. Shen, F. Wang, and Y. Wang, "The sintering mechanism in spark plasma sintering – proof of the occurrence of spark discharge," *Scripta Materialia*, vol. 81, pp. 56 – 59, 2014.

[40] D. Hulbert, A. Anders, J. Andersson, E. Lavernia, and A. Mukherjee, "A discussion on the absence of plasma in spark plasma sintering," *Scripta Materialia*, vol. 60, no. 10, pp. 835 – 838, 2009.

[41] S. Prochazka, *Sintering of Silicon Carbide*, pp. 421–431. Boston, MA: Springer US, 1975.

[42] J. S. Nadeau, "Very high pressure hot pressing of silicon carbide.," *American Ceramic Society Bulletin*, vol. 52, no. 2, pp. 170–174, 1973.

[43] K. Biswas, "Solid state sintering of SiC-ceramics," in *Materials Science Forum*, vol. 624, pp. 71–89, Trans Tech Publ, 2009.

[44] K. Raju and D. Yoon, "Sintering additives for SiC based on the reactivity: A review," *Ceramics International*, vol. 42, no. 16, pp. 17947 – 17962, 2016.

[45] S. Prochazka and R. Scanlan, "Effect of Boron and Carbon on Sintering of SiC," *Journal of the American Ceramic Society*, vol. 58, pp. 72–72, 1 1975.

[46] M. Raczkaa, G. Gornya, L. Stobierskia, and K. Rozniatowskib, "Effect of carbon content on the microstructure and properties of silicon carbide-based sinters," *Materials Characterization*, vol. 46, pp. 245–249, 2001.

[47] V. Suwanmethanond, E. Goo, P. K. T. Liu, G. Johnston, M. Sahimi, and T. T. Tsotsis, "Porous silicon carbide sintered substrates for high-temperature membranes," *Industrial & Engineering Chemistry Research*, vol. 39, no. 9, pp. 3264–3271, 2000.

[48] J. Hojo, *Sintering Behavior of Ultrafine Silicon Carbide Powder*, pp. 149–168. Dordrecht: Springer Netherlands, 1991.

[49] H. Tanaka, *Sintering of Silicon Carbide*, pp. 213–238. Dordrecht: Springer Netherlands, 1991.

[50] W. Van Rijswijk and D. Shanefield, "Effect of Carbon as a Sintering Aid in Silicon Carbide," *Journal of the American Ceramic Society*, vol. 73, pp. 148–149, 1990.

[51] W. J. Clegg, "Role of Carbon in the Sintering of Boron-Doped Silicon Carbide," *Journal of the American Ceramic Society*, vol. 83, pp. 1039–1043, 5 2000.

[52] K. Wiik, *Kinetics of reactions between silica and carbon.* PhD thesis, University of Trondheim, NTH, Trondheim, Norway, 3 1990.

[53] P. Shaffer, "The SiC phase in the system SiC-B4C-C," *Materials Research Bulletin*, vol. 4, no. 3, pp. 213 – 219, 1969.

[54] E. R. Maddrell, "Pressureless sintering of silicon carbide," *Journal of Materials Science Letters*, vol. 6, no. 4, pp. 486–488, 1987.

[55] C. Greskovich and J. H. Rosolowski, "Sintering of covalent solids," *Journal of the American Ceramic Society*, vol. 59, pp. 336–343, 7 1976.

[56] F. F. Lange and T. K. Gupta, "Sintering of sic with boron compounds," *Journal of the American Ceramic Society*, vol. 59, pp. 537–538, 11 1976.

[57] L. Stobierski and A. Gubernat, "Sintering of silicon carbide II. Effect of boron ," *Ceramics International*, vol. 29, no. 4, pp. 355 – 361, 2003.

[58] L. Ogbuji, "Oxidation of polycrystalline silicon carbide," *Ceramics International*, vol. 12, no. 3, pp. 173 – 178, 1986.

[59] A. Maître, A. Put, J. Laval, S. Valette, and G. Trolliard, "Role of boron on the Spark Plasma Sintering of an $\alpha$-SiC powder ," *Journal of the European Ceramic Society*, vol. 28, no. 9, pp. 1881 – 1890, 2008.

[60] Y. Tajima and W. D. Kingery, "Solid solubility of aluminum and boron in silicon carbide," *Journal of the American Ceramic Society*, vol. 65, pp. 27–29, 2 1982.

[61] H. Gu, Y. Shinoda, and F. Wakai, "Detection of boron segregation to grain boundaries in silicon carbide by spatially resolved electron energy−loss spectroscopy," *Journal of the American Ceramic Society*, vol. 82, pp. 469–472, 2 1999.

[62] H. Skarpeid, "Densification of silicon carbide by hot-pressing and the effect of carbon.." Specialisation project, Norwegian University of Science and Technology (NTNU), Trondheim, Norway, 2016.

[63] The International Organization for Standardization (ISO), "ISO 5017:2013." `http://www.iso.org/iso/iso_catalogue/catalogue_tc/catalogue_detail.htm?csnumber=56179`, 2013. [Online; accessed 25-september-2016].

[64] L. Donzel and S. Roberts, "Microstructure and mechanical properties of cubic zirconia (8YSZ)/SiC nanocomposites," *Journal of the European Ceramic Society*, vol. 20, no. 14–15, pp. 2457 – 2462, 2000.

[65] D. Moskovskikh, Y. Lin, A. S. Rogachev, P. J. McGinn, and A. S. Mukasyan, "Spark plasma sintering of SiC powders produced by different combustion synthesis routes," *Journal of the European Ceramic Society*, vol. 35, no. 2, pp. 477 – 486, 2015.

[66] A. K. Suri, C. Subramanian, J. K. Sonber, and T. S. R. C. Murthy, "Synthesis and consolidation of boron carbide: a review," *International Materials Reviews*, vol. 55, no. 1, pp. 4–40, 2010.

[67] W. D. Schaeffer, W. R. Smith, and M. H. Polley, "Structure and properties of carbon black - changes induced by heat treatment," *Industrial & Engineering Chemistry*, vol. 45, no. 8, pp. 1721–1725, 1953.

[68] A. Oberlin, "Carbonization and graphitization," *Carbon*, vol. 22, no. 6, pp. 521 – 541, 1984.

[69] H. N. Murty, D. L. Biederman, and E. Heintz, "Apparent catalysis of graphitization. 3. effect of boron," *Fuel*, vol. 56, no. 3, pp. 305 – 312, 1977.

[70] F. Thévenot, "Boron carbide—a comprehensive review," *Journal of the European Ceramic Society*, vol. 6, no. 4, pp. 205 – 225, 1990.

[71] T. F. Kelly and M. K. Miller, "Atom probe tomography," *Review of Scientific Instruments*, vol. 78, no. 3, pp. 031101 1–18, 2007.

# Appendix A

# Powder

## A.1 Product specification for powder and spray-dried SiC

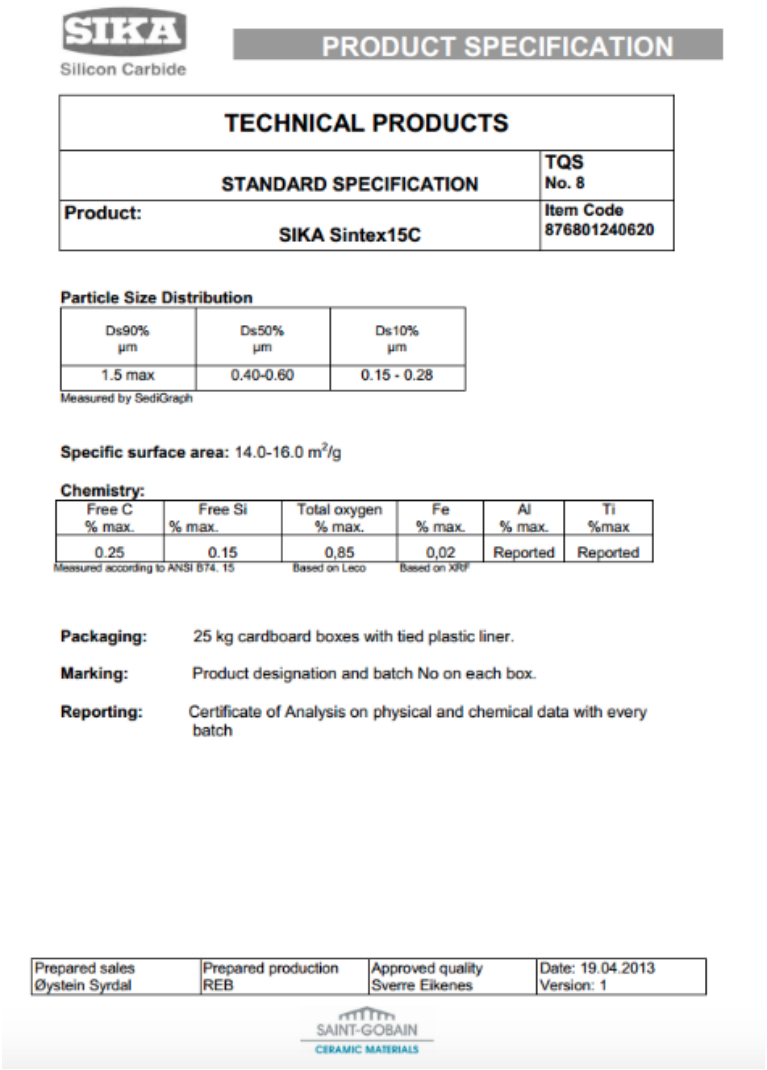

SIKA
Silicon Carbide

PRODUCT SPECIFICATION

| TECHNICAL PRODUCTS | |
|---|---|
| STANDARD SPECIFICATION | TQS No. 8 |
| Product: SIKA Sintex15C | Item Code 876801240620 |

**Particle Size Distribution**

| Ds90% µm | Ds50% µm | Ds10% µm |
|---|---|---|
| 1.5 max | 0.40-0.60 | 0.15 - 0.28 |

Measured by SediGraph

**Specific surface area:** 14.0-16.0 $m^2/g$

**Chemistry:**

| Free C % max. | Free Si % max. | Total oxygen % max. | Fe % max. | Al % max. | Ti %max |
|---|---|---|---|---|---|
| 0.25 | 0.15 | 0,85 | 0,02 | Reported | Reported |

Measured according to ANSI B74. 15 — Based on Leco — Based on XRF

**Packaging:** 25 kg cardboard boxes with tied plastic liner.

**Marking:** Product designation and batch No on each box.

**Reporting:** Certificate of Analysis on physical and chemical data with every batch

| Prepared sales Øystein Syrdal | Prepared production REB | Approved quality Sverre Eikenes | Date: 19.04.2013 Version: 1 |
|---|---|---|---|

SAINT-GOBAIN
CERAMIC MATERIALS

**Figure A.1:** Product specification for SiC powder used before spray drying. Delivered by Development Engineer Benoit Watremetz at Saint-Gobain Ceramic Materials AS Lillesand.

This is the data sheet for Densitec 13H, a ready-to-press (RTP) powder produced by Saint-Gobain. This is similar to Densitec 15H, only a small change in the surface area.

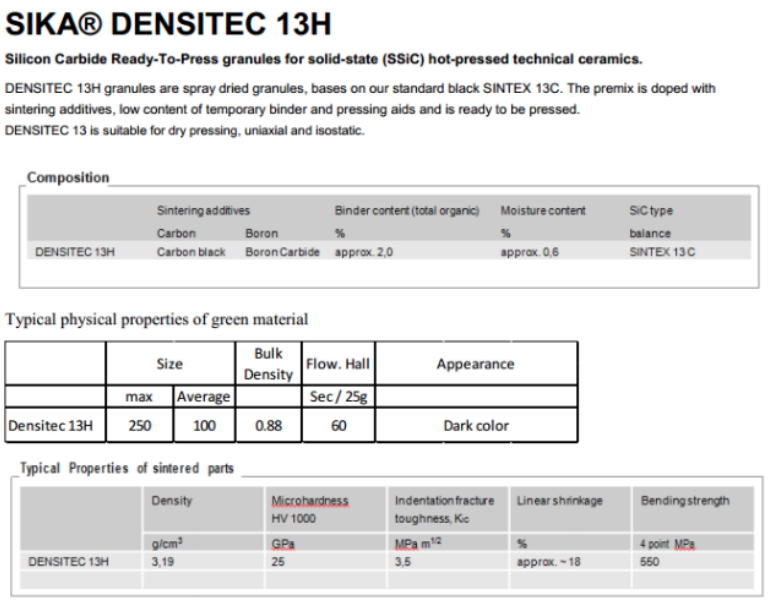

## SIKA® DENSITEC 13H

**Silicon Carbide Ready-To-Press granules for solid-state (SSiC) hot-pressed technical ceramics.**

DENSITEC 13H granules are spray dried granules, bases on our standard black SINTEX 13C. The premix is doped with sintering additives, low content of temporary binder and pressing aids and is ready to be pressed.
DENSITEC 13 is suitable for dry pressing, uniaxial and isostatic.

**Composition**

| | Sintering additives | | Binder content (total organic) | Moisture content | SiC type |
|---|---|---|---|---|---|
| | Carbon | Boron | % | % | balance |
| DENSITEC 13H | Carbon black | Boron Carbide | approx. 2,0 | approx. 0,6 | SINTEX 13 C |

Typical physical properties of green material

| | Size | | Bulk Density | Flow. Hall | Appearance |
|---|---|---|---|---|---|
| | max | Average | | Sec / 25g | |
| Densitec 13H | 250 | 100 | 0.88 | 60 | Dark color |

**Typical Properties of sintered parts**

| | Density | Microhardness HV 1000 | Indentation fracture toughness, Kc | Linear shrinkage | Bending strength |
|---|---|---|---|---|---|
| | g/cm³ | GPa | MPa m$^{1/2}$ | % | 4 point MPa |
| DENSITEC 13H | 3,19 | 25 | 3,5 | approx. ~ 18 | 550 |

**Figure A.2:** Datasheet for Densitec 13H, a ready-to-press (RTP) powder produced by Saint-Gobain. Delivered by Development Engineer Benoit Watremetz at Saint-Gobain Ceramic Materials AS Lillesand.

# Appendix B

# Experimental tests

## B.1 Denisty measurements

The density of isopropanol was calculated from:

$$\rho_{liquid} = -0.0009T + 0.8018 \tag{B.1}$$

The bulk density was calculated from the following equation

$$\rho_b = \frac{m_1}{m_3 - m_2} \cdot \rho_{liquid} \tag{B.2}$$

The apparent porosity was calculated from Equation B.3.

$$\pi_a = \frac{m_3 - m_1}{m_3 - m_2} \cdot 100 \tag{B.3}$$

The true porosity was calculated from Equation B.4.

$$\pi_t = \frac{\rho_t - \rho_b}{\rho_t} \cdot 100 \tag{B.4}$$

The measured densities are listed in Table B.1.

**Table B.1:** Measured densities for the samples with Archemedes' exicator method and and helium pycnometer.

| **Sample** | **Density (A)** [$gcm^{-3}$] | **Open porosity**[%] | **Closed porosity** [%] | **Density (He)** [$gcm^{-3}$] |
|---|---|---|---|---|
| 13CB00 | 3.1702 | 0.4246 | 0.8456 | 3.1550 |
| 13CB0 | 3.1796 | 0.2739 | 0.7053 | 3.2086 |
| 13CB0.3 | 3.1898 | 0.2415 | 0.4190 | 3.2107 |
| 13CB0.8 | 3.1821 | 0.2061 | 0.6934 | 3.2084 |
| 13CB1.0 | 3.1850 | 0.1758 | 0.6329 | 3.1866 |
| 13CB1.5 | 3.1630 | 0.2032 | 1.2918 | 3.1787 |
| 13CB2.5 | 3.1461 | 0.4629 | 1.5580 | 3.1324 |
| 15CB00 | 3.1590 | 0.5300 | 1.0902 | 3.1585 |
| 15CB0 | 3.1719 | 0.4595 | 0.7567 | 3.1940 |
| 15CB0.3 | 3.1795 | 0.4255 | 0.5564 | 3.1924 |
| 15CB0.8 | 3.1846 | 0.6925 | 0.1289 | 3.1977 |
| 15CB1.0 | 3.1787 | 0.4367 | 0.5698 | 3.1972 |
| 15CB1.5 | 3.1773 | 0.1355 | 0.9139 | 3.1832 |
| 15CB2.5 | 3.1487 | 0.3295 | 1.6121 | 3.1383 |
| 13R0.3 | 3.1858 | 0.1133 | 0.6703 | 3.1663 |
| 13R0.8 | 3.1864 | 0.1707 | 0.5968 | 3.1807 |
| 13R1.0 | 3.1800 | 0.1595 | 0.8065 | 3.1957 |
| 13R1.5 | 3.1617 | 0.2617 | 1.2721 | 3.1782 |
| 13B0.2 | 3.1707 | 0.3459 | 0.9096 | 3.1701 |
| 13B0.7 | 3.1520 | 0.3779 | 1.4580 | 3.1459 |
| 13B1.2 | 3.1477 | 0.1833 | 1.7865 | 3.1460 |
| 13B1.7 | 3.1622 | 0.3839 | 1.1355 | 3.1348 |
| 13B0.2 | 3.1713 | 0.3790 | 0.8562 | 3.1806 |
| 13B0.7 | 3.1543 | 0.5338 | 1.2326 | 3.1452 |
| 13B1.2 | 3.1362 | 0.7199 | 1.6090 | 3.1486 |
| 13B1.7 | 3.1563 | 0.7665 | 0.9361 | 3.1421 |
| 13B0.2 | 3.1670 | 0.4014 | 0.9704 | 3.1741 |
| 13B0.7 | 3.1485 | 0.6447 | 1.3032 | 3.1407 |
| 13B1.2 | 3.1370 | 0.6888 | 1.6172 | 3.1483 |
| 13B1.7 | 3.1541 | 0.8232 | 0.9479 | 3.1339 |

## B.2 Phase composition

The amount of the polytypes 4H and 6H, found by structure fittings in Topas, are listed in Tab. B.2 together with the ratio of the polytypes.

**Table B.2:** 4H to 6H ratio as measured by Rietveld fitting in Topas.

| Samples | 4H [%] | 6H [%] | Ratio 4H/6H |
|---|---|---|---|
| 13CB00 | 48.35 | 41.65 | 1.16 |
| 13CB0 | 13.40 | 86.60 | 0.15 |
| 13CB0.3 | 75.72 | 24.29 | 3.12 |
| 13CB0.8 | 55.25 | 44.75 | 1.23 |
| 13CB1.0 | 46.21 | 53.79 | 0.86 |
| 13CB1.5 | 37.32 | 62.68 | 0.60 |
| 13CB2.5 | 36.34 | 63.66 | 0.57 |
| 15CB00 | 43.62 | 56.38 | 0.77 |
| 15CB0 | 17.51 | 82.49 | 0.21 |
| 15CB0.3 | 18.46 | 81.54 | 0.23 |
| 15CB0.8 | 16.60 | 86.40 | 0.19 |
| 15CB1.0 | 15.38 | 84.62 | 0.18 |
| 15CB1.5 | 11.12 | 88.88 | 0.13 |
| 15CB2.5 | 14.50 | 85.50 | 0.17 |
| 13R0.3 | 53.56 | 46.44 | 1.15 |
| 13R0.8 | 47.83 | 52.17 | 0.92 |
| 13R1.0 | 34.38 | 65.62 | 0.52 |
| 13R1.5 | 92.50 | 7.50 | 12.33 |
| 13B0.2 | 14.60 | 85.40 | 0.17 |
| 13B0.7 | 19.78 | 80.22 | 0.25 |
| 13B1.2 | 21.79 | 78.21 | 0.28 |
| 13B1.7 | 4.31 | 95.69 | 0.05 |

## B.3 Mechanical properties

The measured hardness of each sample are listed in Tab. B.4, Tab. B.3 and Tab. B.5. The average hardness calculated from indents and fracture toughness calculated from indent size and crack propagating from these indents can be found in Tab. B.6.

**Table B.3:** Hardness value measured with Vickers micro-indentation with a load of 1 kg. The values are given in HV. These numbers are from work conducted by Skarpeid[62].

| Sample # | 13CB0.3 | 13CB0.8 | 13CB1.0 | 13CB1.5 | 15CB0.3 | 15CB0.8 | 15CB1.0 | 15CB1.5 |
|---|---|---|---|---|---|---|---|---|
| 1 | 2739 | 2956 | 2990 | 2651 | 2499 | 3053 | 2942 | 2841 |
| 2 | 2770 | 2751 | 2939 | 2734 | 2775 | 2622 | 2745 | 2736 |
| 3 | 2548 | 2997 | 2966 | 2622 | 2949 | 2714 | 3005 | 2757 |
| 4 | 2594 | 3145 | 2915 | 2818 | 2939 | 2965 | 2922 | 2893 |
| 5 | 2685 | 2508 | 3119 | 2698 | 2704 | 2514 | 3025 | 2942 |
| 6 | 2866 | 3001 | 2907 | 2606 | 2838 | 2840 | 2874 | 2908 |
| 7 | 2406 | 3020 | 3179 | 2777 | 2621 | 2764 | 2836 | 2671 |
| 8 | 2705 | 3045 | 2902 | 2700 | 2550 | 2780 | 2660 | 2841 |
| 9 | 2723 | 2791 | 2783 | 2689 | 2536 | 2642 | 2874 | 2943 |
| 10 | 2566 | 2844 | 2974 | 2622 | 2805 | 2969 | 2801 | 2796 |

**Table B.4:** Hardness value measured with Vickers micro-indentation with a load of 1 kg. The values are given in HV.

| Sample Measurement | 13CB00 | 13CB0 | 13CB2.5 | 15CB00 | 15CB0 | 15CB2.5 |
|---|---|---|---|---|---|---|
| 1 | 2963 | 2766 | 2436 | 2828 | 2691 | 2982 |
| 2 | 2673 | 2863 | 2548 | 2677 | 2521 | 2796 |
| 3 | 2759 | 2644 | 2476 | 2592 | 2672 | 2730 |
| 4 | 2827 | 2897 | 2328 | 2683 | 2836 | 2803 |
| 5 | 2820 | 3060 | 2854 | 2747 | 2825 | 2825 |
| 6 | 2681 | 2675 | 2604 | 2897 | 2567 | 2905 |
| 7 | 2703 | 2784 | 2772 | 2737 | 2742 | 2726 |
| 8 | 2643 | 2856 | 2631 | 2764 | 2773 | 2871 |
| 9 | 2637 | 2793 | 2616 | 2729 | 2942 | 2852 |
| 10 | 2654 | 2883 | 2468 | 2656 | 2735 | 2618 |

**Table B.5:** Hardness value measured with Vickers micro-indentation with a load of 1 kg. The values are given in HV.

| Sample / Measurement | 13R0.3 | 13R0.8 | 13R1.0 | 13R1.5 | 13B0.2 | 130.7 | 13B1.2 | 13B1.7 |
|---|---|---|---|---|---|---|---|---|
| 1 | 2854 | 2911 | 2877 | 2633 | 2521 | 3484 | 2498 | 2952 |
| 2 | 2469 | 3056 | 2691 | 2818 | 2569 | 2946 | 2397 | 2775 |
| 3 | 2713 | 2844 | 2671 | 2740 | 2665 | 2870 | 3018 | 2717 |
| 4 | 2929 | 2920 | 2750 | 2587 | 2708 | 2715 | 2871 | 2796 |
| 5 | 2798 | 2680 | 2873 | 2612 | 2649 | 2915 | 3181 | 2793 |
| 6 | 2874 | 2816 | 2654 | 3174 | 2702 | 3281 | 2881 | 2814 |
| 7 | 2689 | 2899 | 2857 | 2755 | 2726 | 2765 | 2728 | 2867 |
| 8 | 2646 | 2798 | 2650 | 2909 | 2524 | 2608 | 2873 | 2692 |
| 9 | 2905 | 2793 | 2751 | 2751 | 2628 | 2745 | 2968 | 2771 |
| 10 | 2842 | 2646 | 2464 | 2571 | 2719 | 2902 | 2869 | 2794 |

**Table B.6:** The average hardness and fracture toughness calculated from indent size and cracks propagating from the indents.

| Samples | Hardness [HV] | Fracture toughness [MPa$\sqrt{\text{m}}$] |
|---|---|---|
| 13CB00 | 3094 | 1.51 |
| 13CB0 | 2945 | 1.40 |
| 13CB0.3 | 2696 | 4.52 |
| 13CB0.8 | 3164 | 4.63 |
| 13CB1.0 | 3589 | 4.39 |
| 13CB1.5 | 3235 | 3.20 |
| 13CB2.5 | 3007 | 2.15 |
| 15CB00 | 2875 | 2.09 |
| 15CB0 | 3166 | 2.42 |
| 15CB0.3 | 2966 | 3.32 |
| 15CB0.8 | 2680 | 2.59 |
| 15C31.0 | 2920 | 2.07 |
| 15CB1.5 | 3140 | 2.33 |
| 15CB2.5 | 2895 | 2.23 |
| 13R0.2 | 2969 | 2.32 |
| 13R0.8 | 2885 | 2.69 |
| 13R1.0 | 2928 | 2.64 |
| 13R1.5 | 2752 | 2.21 |
| 13B0.2 | 2889 | 2.13 |
| 13B0.7 | 3151 | 2.06 |
| 13B1.2 | 4302 | 2.13 |
| 13B1.7 | 3090 | 2.04 |

# Appendix C

# Scanning electron microscopy images

Images of samples taken with Scanning electron microscope(SEM) can be found here. Fracture images can be seen in Fig. C.1 and Fig. C.2. Fig. C.3, Fig. C.4, Fig. C.5 and Fig. C.6 show images of two indents per sample. Images of the microstructure of the samples tested in the specialisation project can be found in Fig. 4.1 and Fig. 4.2.

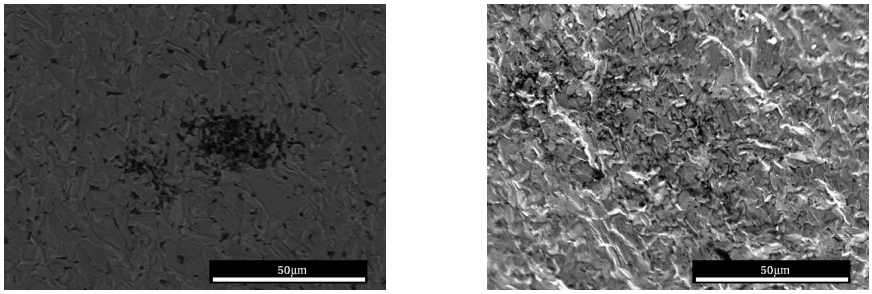


**(a)** 13CB2.5 **(b)** 15CB2.5

**Figure C.1:** SEM-images of fracture surfaces showing either carbon rich or porous areas in the samples with 2.5wt.% carbon black

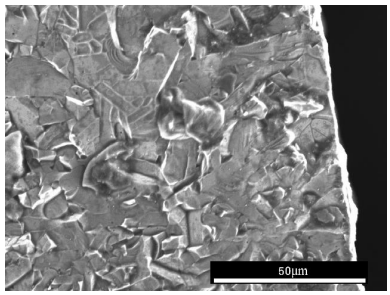


**(a)** 13CB0.3

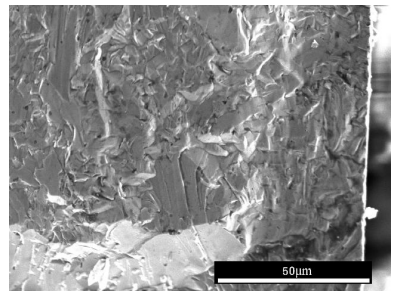


**(b)** 15CB0.3

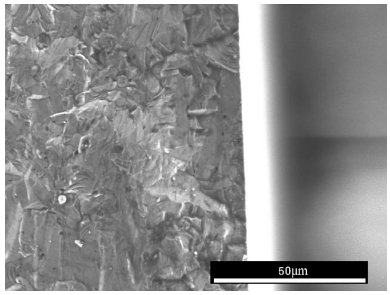


**(c)** 13CB0.8

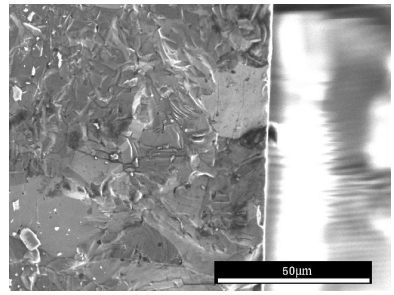


**(d)** 15CB0.8

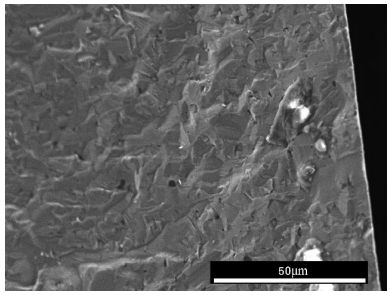


**(e)** 13CB1.0

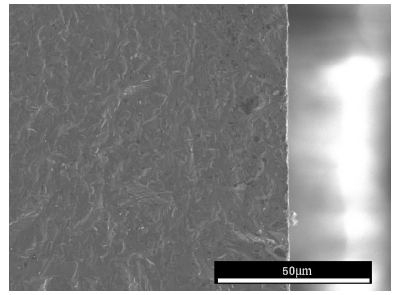


**(f)** 15CB1.0

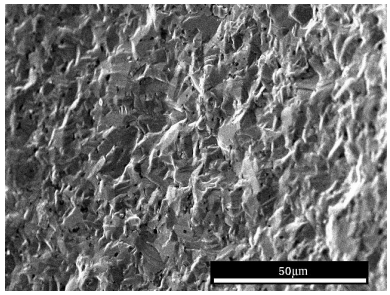


**(g)** 13CB1.5

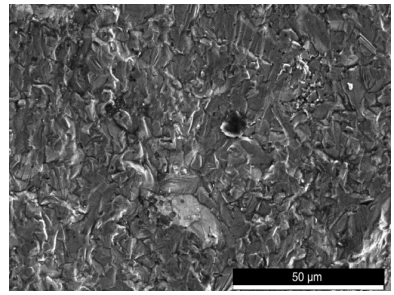


**(h)** 15CB1.5

**Figure C.2:** SEM-images of fracture surfaces from Skarpeid[62].

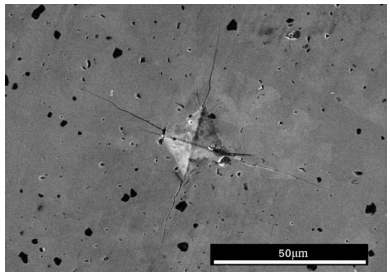


**(a)** 13R0.3

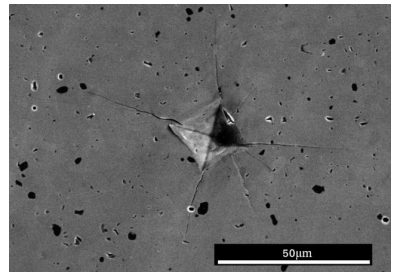


**(b)** 13R0.3

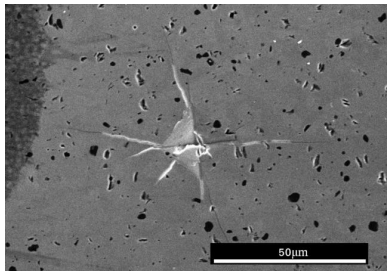


**(c)** 13R0.8

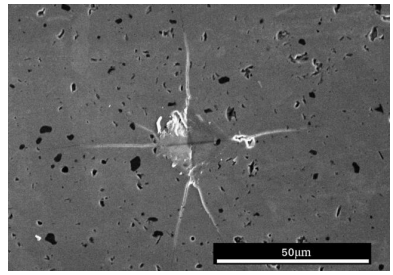


**(d)** 13R0.8

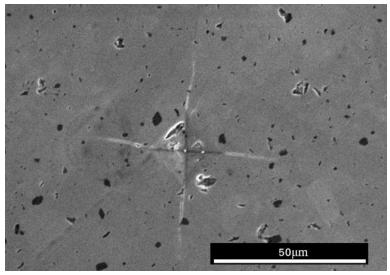


**(e)** 13R1.0

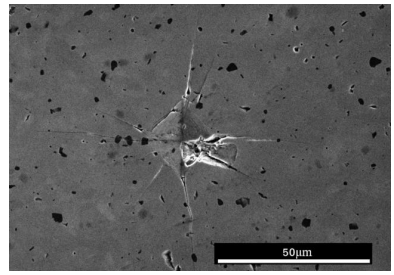


**(f)** 13R1.0

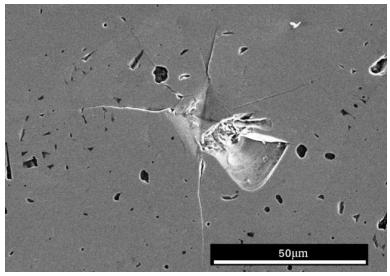


**(g)** 13R1.5

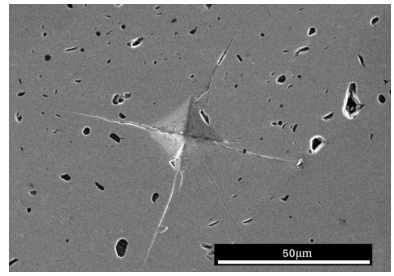


**(h)** 13R1.5

**Figure C.3:** SEM-images of some of the indents taken of the hot-pressed sample with variation in resin content.

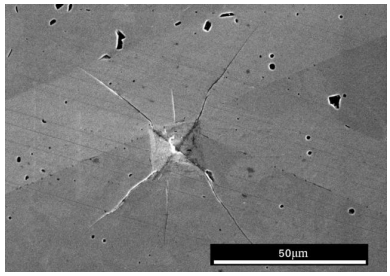


**(a)** 13B0.2

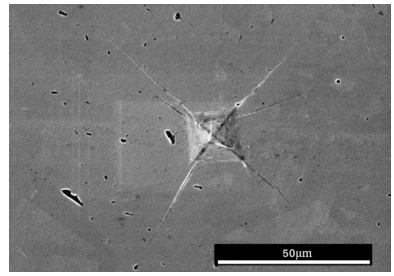


**(b)** 13B0.2

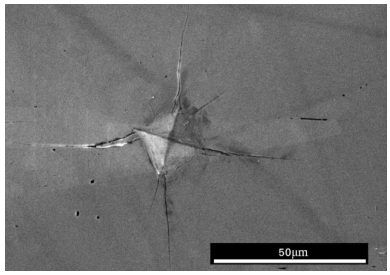


**(c)** 13B0.7

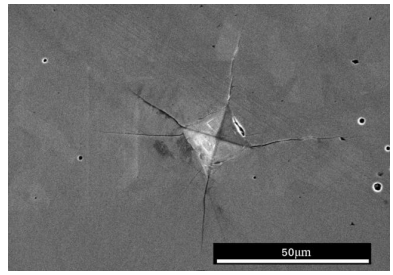


**(d)** 13B0.7

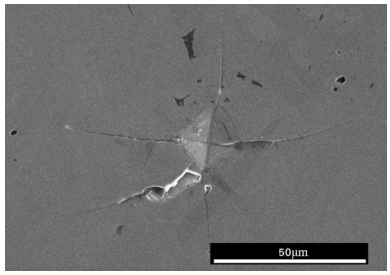


**(e)** 13B1.2

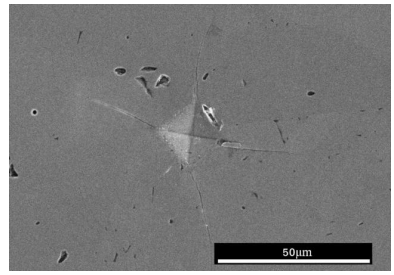


**(f)** 13B1.2

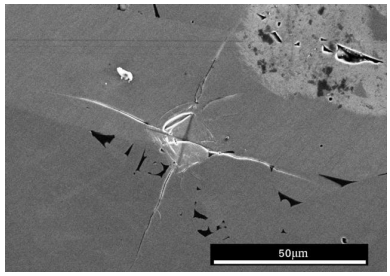


**(g)** 13B1.7

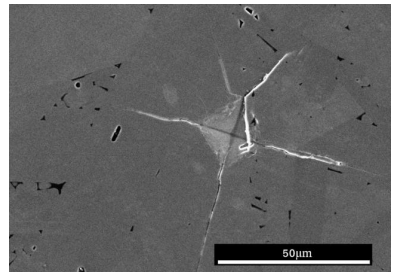


**(h)** 13B1.7

**Figure C.4:** SEM-images of some of the indents taken of the spark plasma sintered samples with variation in boron carbide content.

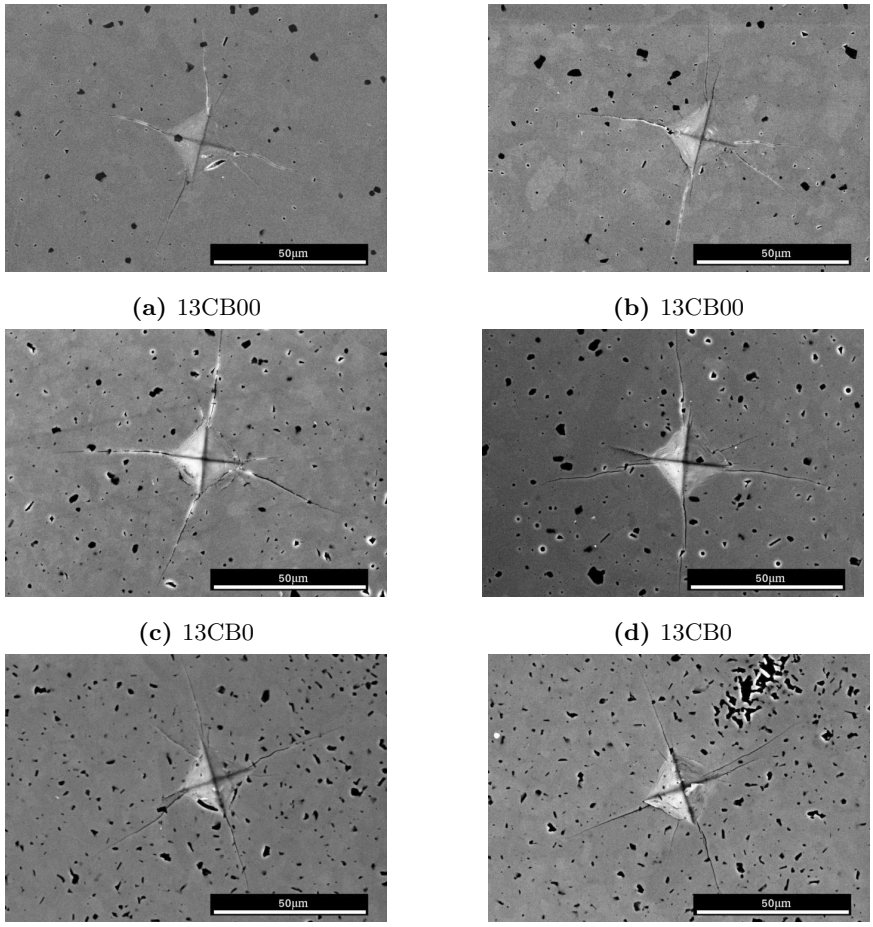


**(a)** 13CB00 **(b)** 13CB00

**(c)** 13CB0 **(d)** 13CB0

**(e)** 13CB2.5 **(f)** 13CB2.5

**Figure C.5:** SEM-images of some of the indents taken of the hot-pressed samples with variation in carbon black content and a specific surface area of $13m^2g^{-1}$.

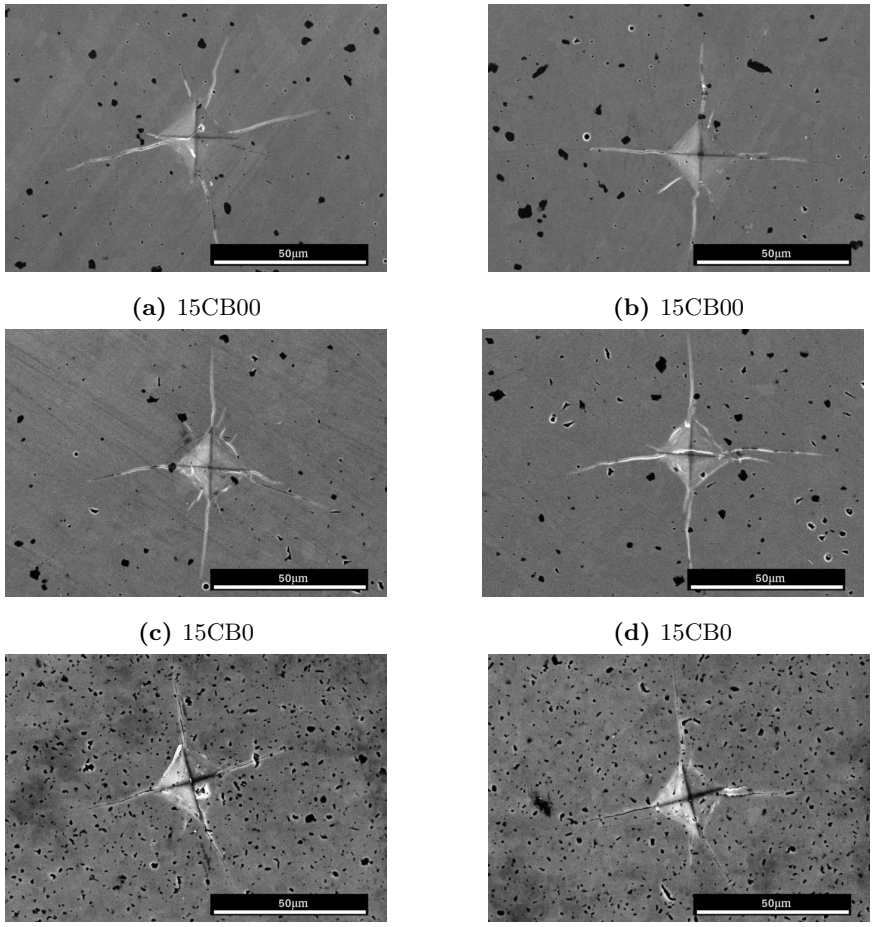


**(a)** 15CB00 **(b)** 15CB00

**(c)** 15CB0 **(d)** 15CB0

**(e)** 15CB2.5 **(f)** 15CB2.5

**Figure C.6:** SEM-images of some of the indents taken of the hot-pressed samples with variation in carbon black content and a specific surface area of $15m^2g^{-1}$.

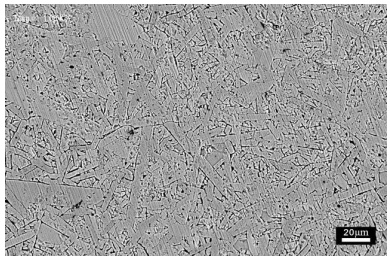


**(a)** 13CB0.3

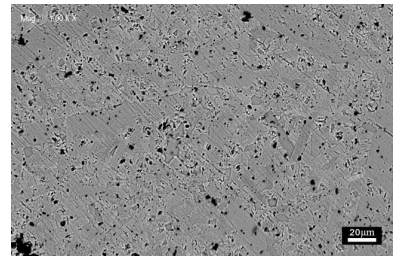


**(b)** 13CB0.8

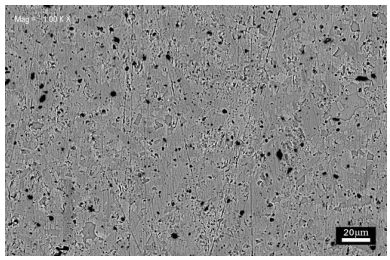


**(c)** 13CB1.0

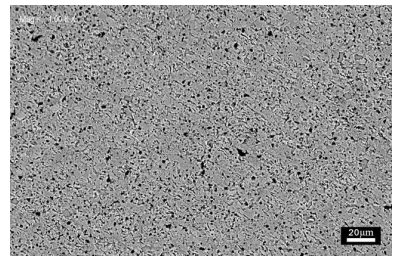


**(d)** 13CB1.5

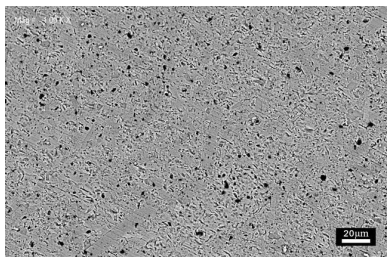


**(e)** 15CB0.3

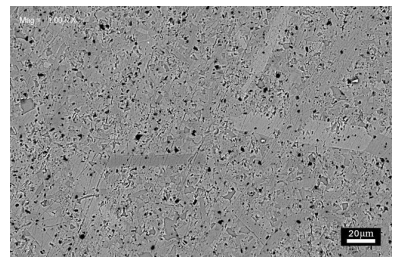


**(f)** 15CB0.8

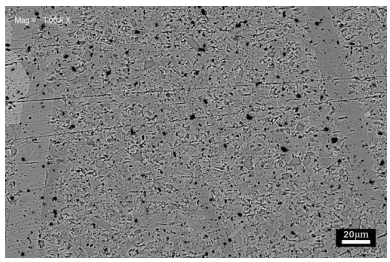


**(g)** 15CB1.0

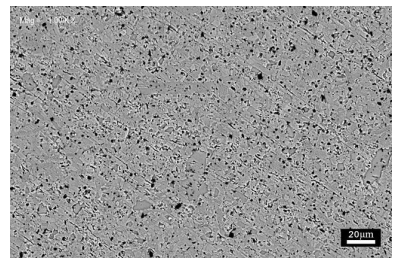


**(h)** 15CB1.5

**Figure C.7:** SEM-images (BSD) of microstructures taken of hot-pressed samples with carbon black content from 0.3-1.5wt.% by Skarpeid[62].

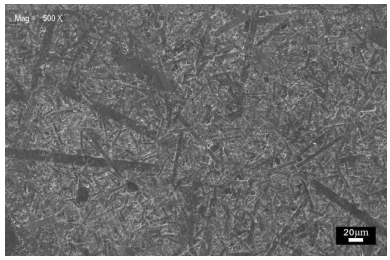


**(a)** 13CB0.3

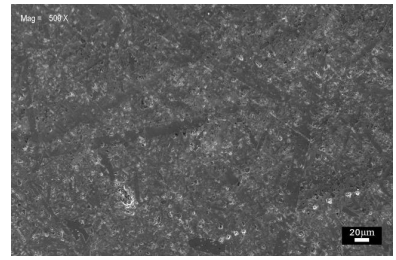


**(b)** 13CB0.8

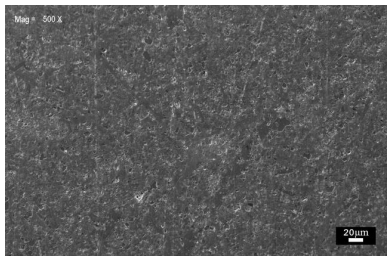


**(c)** 15CB1.0

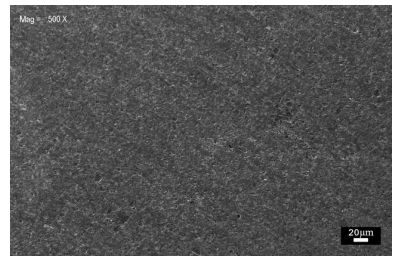


**(d)** 13CB1.5

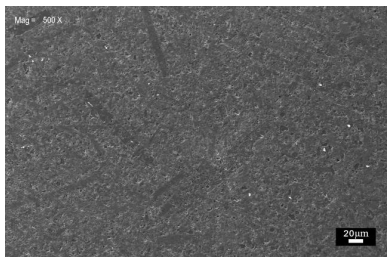


**(e)** 15CB0.3

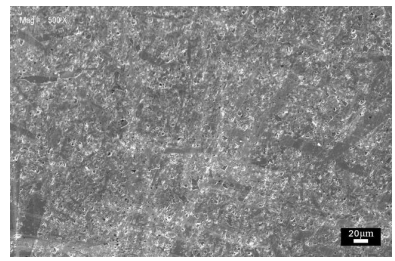


**(f)** 15CB0.8


**(g)** 15CB1.0

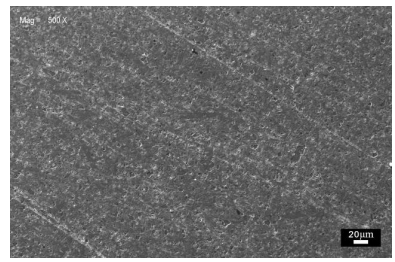


**(h)** 15CB1.5

**Figure C.8:** SEM-images(SE) of microstructures taken of hot-pressed samples with carbon black content from 0.3-1.5wt.% by Skarpeid[62].